Eno schemes on unstructured meshes

Remi Abgrall, Frédéric C. Lafon

INRIA

INSTITUT NATIONAL DE RECHERCHE EN INFORMATIQUE ET EN AUTOMATIQUE

Eno Schemes on Unstructured Meshes

Rémi ABGRALL
Frédéric C. LAFON

N° 2099
Novembre 1993

PROGRAMME 6

Calcul scientifique,
modélisation et
logiciels numériques

ENO SCHEMES ON UNSTRUCTURED MESHES

Rémi Abgrall*, Frédéric C. Lafon **

Programme 6 — Calcul scientifique, modélisation et logiciel numérique
Projet Sinus

Abstract: This material represents the notes of a lecture made during the Lecture Series Programme, Computational Fluid held at the von Kàrman Institute in April 1993. We present the ENO methods in the context of the finite volume methods. Then we show how to extend them to multidimensional problems, in particular when the mesh become unstructured. We also discuss the different methods and give numerical illustrations.

(Résumé : tsvp)

Cours au von Kàrman Institute (Bruxelles, Belgique). Lecture Series in Computational Fluid Dynamic, April 1993

*INRIA, BP 93, 06902 Sophia Antipolis Cedex, France
**CEA, Centre de Limeil-Valenton, 94195 Villeuneuve St Georges, France

Unité de recherche INRIA Sophia-Antipolis
2004 route des Lucioles, BP 93, 06902 SOPHIA-ANTIPOLIS Cedex (France)
Téléphone : (33) 93 65 77 77 – Télécopie : (33) 93 65 77 65

SCHEMAS ENO SUR MAILLAGES NON STRUCTURES

Résumé : Ce texte représente les notes écrites d'un cours effectué dans le cadre des "Lecture Series Programme, Computational Fluid Dynamics" de l'Institut von Kàrman de Bruxelles en Avril 1993. On expose la théorie des schémas ENO dans le cadre des méthodes volumes finis. Ensuite on montre diverses généralisations de ces méthodes à des problèmes multidimensionnels, en particulier quand le maillage devient non structuré. On compare aussi ces dernières et on donne des exemples de simulations numériques.

ENO schemes on Unstructured Meshes

R. Abgrall[♣] & F.C. Lafon[♠]
♣ INRIA, BP 93, 06902 Sophia Antipolis Cedex, France
abgrall@sophia.inria.fr
♠ CEA, Centre de Limeil-Valenton, 94195 Villeuneuve St Georges, France
lafon@glaieul.saclay.cea.fr

1 Introduction

During the past few years, a growing interest has emerged for building high order accurate and robust schemes for compressible flows simulations. One of the difficulties is the appearance of possibly strong discontinuities that may interact together, even for smooth initial data. To get rid of this difficulty, a possible solution is to use a Totally Variation Diminishing scheme. Such a scheme has the property, at least for 1D scalar equation, not to create new extrema, and hence to provide a nice treatment of discontinuities. They have been since successfully and widely used with any type of meshes (see for example, [1] for a review and, among many others, [2] for simulations on finite elements type meshes and [3] for simulations for moving boundary problems). They are now of common use even for industrial simulations on complex geometries. Nevertheless, one of their main weakness is that the order of accuracy falls to first order in regions of discontinuity and at extrema, leading to excessive numerical dissipation.

Various methods have been proposed to overcome this difficulty (adaptation of the mesh, for example see [4, 5, 6]) but one promising way may also be the class of the Essentially Non-Oscillatory schemes (E.N.O. for short) introduced by Harten, Osher and others [7, 8, 9, 10, 11].

The basic idea of E.N.O schemes is to use a Lagrange type interpolation with an adapted stencil : when a discontinuity is detected, the procedure looks for the region around this discontinuity where the function is the smoothest. This reconstruction technique may be applied either to the node values [10] or to a particular function constructed averages in control volumes [7, 8, 9]. In this latter case, the approximation is done in such a way that it is conservative. This enables to approximate any piecewise smooth function at any desired order of accuracy.

The purpose of this lecture is twofolds : first to provide a description of the basic ideas of the "classical" ENO methods, and second to show how it is possible to adapt them on general geometries. Because of the lack of space and the personal experience of the authors, it is not possible to provide a complete overview of ENO methods. Hence, this lecture will concentrate on finite volumes ENO methods and triangular types meshes. Nevertheless, we believe that it will provide the most typical features of ENO methods on general geometries, and the difficulties of the problem.

This lecture is organized as follow : we first recall the principle of finite volume schemes. This enable us to show the three steps of a finite volume scheme : the reconstruction step, the evolution step and the projection step. Generally, the last two steps are merged together by means of Riemann solver and an appropriate temporal scheme. Before entering in the main topic of this lecture, the

reconstruction step, we give several Runge-Kutta methods due to Shu and Osher that enable to keep the TVD or TVB features of the first order approximation of a generalized Riemann problem with non constant datas. Then we move to the reconstruction problem. First, we detail the "classical" methods that are applied to real valued functions and show why it cannot be applied on general geometries. We also discuss some pathologies of ENO reconstruction procedures and how to cure the problems. These pathologies may have some common points with the analysis of [31] on second order upwind schemes. To overcome this difficulty, we introduce a new reconstruction procedure first introduced by Barth [17]. We give and show its properties that appears to be the same than those of a more classical Lagrange reconstruction.

2 An overview of finite volume schemes

In order to set up the context of this lecture, we discuss the main ingredients of the finite volume schemes on a 1D scalar equation. In a further section, we discuss the additional approximation that have to be made for multidimensional problems.

Let us consider the following equation

$$\frac{\partial u}{\partial t} + \frac{\partial f(u)}{\partial t} = 0 \tag{1}$$

for $t > 0$, with additional initial conditions :

$$u(x, t = 0) = u_0(x). \tag{2}$$

We assume f to be convex, of class C^2 and u_0 to be regular enough, say $||u_0||_\infty < +\infty$, $u_0 \in L^1(\mathbb{R})$ and of bounded variation. We also assume that there exists an entropy, that is a convex function $U(u)$ such there exists an entropy flux $F(u)$ with

$$U'(u)\ f'(u) = F'(u). \tag{3}$$

We impose the entropy condition :

$$\frac{\partial U(u)}{\partial t} + \frac{\partial F(u)}{\partial t} \leq 0 \tag{4}$$

that must fulfill the solution u.

The classical theory on 1D conservative equation can be applied (see for example [26] for a tutorial) :

1. There exists a unique entropy solution to problem (1-2-4) denoted by $E[u_0]$,
2. For any $t \geq 0$, $||E[u_0](\ .\ , t)||_\infty \leq ||u_0||_\infty$,
3. $TV(E[u_0](\ .\ , t)) \leq TV(u_0)$ for all $t \geq 0$,
4. $\int_{\mathbb{R}} |E[u_0](x, t_2) - E[u_0](x, t_1)|dx \leq C\ TV(u_0)|t_2 - t_1|$, for all $t_2, t_1 \geq 0$

As usual, we have adopted the following notations :

- $||u||_\infty$ is the minimum of the constants C such that $|u(x)| \leq C$ almost everywhere,

- $TV(u)$ is defined by :

$$TV(u) = sup\{\int_{\mathbb{R}} u\ \phi' dx, \phi \in C_0^1(\mathbb{R}), ||\phi||_\infty \leq 1\}$$

If u lies in C^1 then $TV(u) = \int_{\mathbb{R}} |u'| dx$. If u is constant by parts :

$$u(x) = u_i \quad \text{if} \quad x_i < x \leq x_{i+1}$$

((x_i) is a subdivision of $\mathbb{R}$) then $TV(u) = \sum_i |u_{i+1} - u_i|$. If now, for the same subdivision, u is polynomial by parts :

$$u(x) = P_i(x) \quad \text{if} \quad x_i < x \leq x_{i+1}$$

where (P_i) is a set of polynomial of degree $\leq k$, then

$$TV(u) = \sum_i \int_{x_i}^{x_{i+1}} |P_i'(x)| dx + \sum_i |P_i(x_{i+1}) - P_{i+1}(x_i + 1)|$$

and so on.

Let us give a sequence of increasing elements of $\mathbb{R}$, denoted as $(x_{i+1/2})$. For example, if (x_i) is an other subdivision of $\mathbb{R}$ (a "mesh"), we may state :

$$x_{i+1/2} = \frac{x_i + x_{i+1}}{2}.$$

It is well known that if one integrates equation (1) in $[x_{i-1/2}, x_{i+1/2}] \times [t_1, t_2]$, with the notation :

$$\overline{u}_i(t) = \frac{\int_{x_{i-1/2}}^{x_{i+1/2}} u(x,t) dx}{x_{i+1/2} - x_{i-1/2}},$$

one gets

$$\overline{u}_i(t_2) - \overline{u}_i(t_1) + (x_{i+1/2} - x_{i-1/2}) \left[\int_{t_1}^{t_2} f(u(x_{i+1/2}, s) ds - \int_{t_1}^{t_2} f(u(x_{i-1/2}, s) ds \right] = 0 \qquad (5)$$

The set $[x_{i-1/2}, x_{i+1/2}]$ is called a control volume.

Let us describe now the principle of any finite volume scheme. For the sake of simplicity, we assume a constant time step Δt so that one looks for an approximation (u_i^n) of the true solution $E[u_0]$ of the problem (1-2) at times $t_n = n\Delta t, n \geq 0$. From equation (5), we see that a finite volume scheme is constructed as follows :

1. *At $t = 0$, the initial condition is approximated by its averages on the control volumes $[x_{i-1/2}, x_{i+1/2}]$,*
2. *Getting (u_i^{n+1}) from (u_i^n) can be achieved in three steps :*
   - **a- Reconstruction step** : *from the u_i^n's, compute for the interval $[x_{i-1/2}, x_{i+1/2}]$ a polynomial P_i that approximates "well" $E[u_0]$ at time t_n in that interval.*
   - **b- Evolution step** : *apply the evolution operator E to the function R_n defined locally by the P_i's,*

c- **Projection step** : *Evaluate the averages of the function* $E[R_n]$ *at time* t_{n+1} *in the control volume. The result is* u_i^{n+1}.

The steps (b) and (c) can be merged in a same step by mean of the formula (5) where u has been replaced by $E[R_n]$.

In (a), the word "well" has not been clearly defined. It is natural to ask for the following properties [7, 8, 9] for a reconstruction $R(u,k)$ of degree k :

P1 *If* u *is of class* C^r *with* $r \geq k$, *then the* $l-th$ *order derivative of* $u - R(u,k)$, $l \leq k$ *satisfies* $u^{(l)} - R(u,k)^{(l)} = O(h^{k+1-l})$,

P2 $TV(R(u,k)) \leq TV(u) + O(h^r)$,

P3 *The average of* $R(u,k)$ *over* $[x_{i-1/2}, x_{i+1/2}]$ *is equal to that of* u.

The property 1 guaranties the accuracy of the approximation. The property 2 guaranties (for reasonable flux functions) that the scheme is Total variation Bounded and hence converges to the correct solution for any $t \in [0,T]$. The property 3 states the consistency of the scheme. Before entering into the details of the reconstruction step, let us briefly comment the evolution operator.

3 Approximation of the evolution operator

In general, the evolution operator is not exactly known so that step (b) is generally replaced by an approximated one. A convenient way of doing this can be obtained with the method of lines : instead of integrating equation (1) in $[x_{i-1/2}, x_{i+1/2}] \times [t_1, t_2]$, we only integrate in space with the initial condition $R(u,k)$:

$$\frac{\partial \overline{u}_i}{\partial t} = -\frac{1}{x_{i+1/2} - x_{i-1/2}} \left(f(E[R(u,k)](x_{i+1/2}, t^+)) - f(E[R(u,k)](x_{i+1/2}, t^+)) \right) \simeq L[R(u,k)] \quad (6)$$

where $E[R(u,k)](x_{i+1/2}, t^+) = \lim_{\substack{s \to t \\ s > t}} E[R(u,k)](x_{i+1/2}, s)$ for $x_{i+1/2}$ and a similar expression for $x_{i-1/2}$. Then, one approximates $f(E[R(u,k)](x_{i+1/2}, t^+))$, for example, with the help of any suitable Riemann solver, and the equation (6) is rewritten and approximated like

$$\frac{\partial \overline{u}_i}{\partial t} = \mathcal{L}_i[u] \quad (7)$$

A classical way of solving this set of ordinary differential equations is to use a Runge Kutta scheme. Among these schemes, some of them have the property not to increase the total variation [10]. They are built as follows. Consider a general Runge-Kutta scheme :

$$\begin{aligned} & u^{(i)} = u^{(0)} + \Delta t \sum_{k=0}^{i-1} c_{ik} \mathcal{L}(u^{(k)}, t^n + d_k \Delta t), \quad i = 1, 2, \cdots m \\ & u(0) = u^n, \qquad u^{(m)} = u^{n+1} \end{aligned} \quad (8)$$

where $d_k = \sum_{i=0}^{k-1} c_{ik}$. Let us consider a sequence (α_{ik}) such that $\alpha_{ik} \geq 0$ and $\sum_{k=0}^{i-1} \alpha_{ik} = 1$. Then one can rewrite this Runge-Kutta scheme as :

$$u^{(i)} = \sum_{k=0}^{i-1} \left[\alpha_{ik} + \beta_{ik}\ \Delta t \mathcal{L}(u^{(k)})\right]$$

One gets the following result :

Proposition 3.1 *Assume that the schemes*

$$w = (Id + \Delta t \mathcal{L})(u) \quad \text{and} \quad w = (Id - \Delta t \tilde{\mathcal{L}})(u),$$

(where $\tilde{\mathcal{L}}$ is an approximation of $-L$) are TVD under the condition $\Delta t \leq \Delta t_0$, we get the results :

1. *if all the β_{ik} are positive and $\Delta t \leq \Delta t_0 \min_{i,k} \frac{\alpha_{ik}}{|\beta_{ik}|}$, then the scheme (8) is TVD. Note that the condition on $\tilde{\mathcal{L}}$ does not play any role.*
2. *if one of the $\beta_{i_0 k_0}$ is negative, when one replace $\mathcal{L}$ by $\tilde{\mathcal{L}}$, the same conclusion holds under the same condition.*

Before giving examples of such Runge-Kutta schemes, let us explain, for the Roe's linearization, this mysterious $\tilde{\mathcal{L}}$. Consider a linear hyperbolic equation $U_t + AU_x = 0$ and omitting the reconstruction operator of equation (6), one has

$$L[u] \simeq \frac{1}{2}[AU_{i+1} + AU_i - |A|(U_{i+1} - U_i)] - \frac{1}{2}[AU_i + AU_{i-1} - |A|(U_i - U_{i-1})]$$

An approximation for the equation $U_t - AU_x = 0$ is then given by

$$\tilde{\mathcal{L}}[u] \simeq \frac{1}{2}[-AU_{i+1} - AU_i - |A|(U_{i+1} - U_i)] - \frac{1}{2}[-AU_i - AU_{i-1} - |A|(U_i - U_{i-1})].$$

The upwinding is made in the opposite direction.

Some examples :

1. **Second order scheme** : the classical Heun's method. It is TVD under the condition $\Delta t \leq \Delta t_0$ (CFL=1).

$$u^{(1)} = u^{(0)} + \Delta t \mathcal{L}(u^{(0)})$$

$$u^{(2)} = \tfrac{1}{2}u^{(0)} + \tfrac{1}{2}u^{(1)} + \tfrac{1}{2}\mathcal{L}(u^{(1)})$$

2. **Third order scheme, TVD under CFL=1 :**

$$u^{(1)} = u^{(0)} + \Delta t \mathcal{L}(u^{(0)})$$

$$u^{(2)} = \tfrac{3}{4}u^{(0)} + \tfrac{1}{4}\left(u^{(1)} + \Delta t \mathcal{L}(u^{(1)})\right)$$

$$u^{(3)} = \tfrac{1}{3}u^{(0)} + \tfrac{2}{3}\left(u^{(2)} + \Delta t \mathcal{L}(u^{(2)})\right)$$

3. **Fourth order scheme** : It is not possible [10] to get rid off $\tilde{\mathcal{L}}$ this time. This scheme is TVD under CFL=2/3. It is the TVD version of the classical fourth order Runge-Kutta method.

$$u^{(1)} = u^{(0)} + \tfrac{1}{2}\Delta t\mathcal{L}(u^{(0)})$$

$$u^{(2)} = \tfrac{1}{2}u^{(0)} - \tfrac{1}{4}\Delta t\tilde{\mathcal{L}}(u^{(0)}) + \tfrac{1}{2}u^{(1)} + \tfrac{1}{2}\Delta t\mathcal{L}(u^{(1)})$$

$$u^{(3)} = \tfrac{1}{9}u^{(0)} - \tfrac{1}{9}\Delta t\tilde{\mathcal{L}}(u^{(0)}) + \tfrac{2}{9}u^{(1)} - \tfrac{1}{3}\Delta t\tilde{\mathcal{L}}(u^{(1)}) + \tfrac{2}{3}u^{(2)} + \Delta t\mathcal{L}(u^{(2)})$$

$$u^{(4)} = \tfrac{1}{3}u^{(1)} + \tfrac{1}{6}\Delta t\mathcal{L}(u^{(1)}) + \tfrac{1}{3}u^{(2)} + \tfrac{1}{3}u^{(3)} + \tfrac{1}{6}\mathcal{L}(u^{(3)})$$

Until the end of this lecture, we will not give more details on the time stepping since our purpose is to concentrate on the reconstruction step of a finite volume scheme. For that reason, all the numerical examples that illustrates this lecture are obtained with one of the above time stepping.

Remark : The Runge-Kutta schemes are easy to implement but, to recover the expected order of accuracy, the reconstruction procedure must be performed at each sub-steps. To avoid this, one may use a Cauchy-Kowaleska procedure as Harten where only one reconstruction per time step is needed, but the implementation is much more complex.

4 The reconstruction step : classical methods

4.1 An example

It is known that if one tries to interpolate a discontinuous function with a fixed stencil, the approximation may be very bad due to the Gibbs-like phenomenon. As an example, let us consider the Heaviside function H :

$$H(x) = \begin{cases} 1 & \text{if } x \leq 0 \\ -1 & \text{else} \end{cases}$$

that we try to interpolate on the mesh $x_i = \Delta x, i \in \mathbf{Z}$ with a fixed central stencil : on $[x_{i-1/2}, x_{i+1/2}]$, we use the points x_{i-1}, x_i and $x_{i+1/2}$. Let us denote by R the function that coincides on the interval $[x_{i-1/2}, x_{i+1/2}]$ with the Lagrange interpolation with this central stencil. This gives :

$$R(x) = \begin{cases} 1 & \text{if } x < -\frac{\Delta x}{2} \\ -1 & \text{if } x > -\frac{\Delta x}{2} \\ \frac{13}{12} - \frac{x}{\Delta x} - (\frac{x}{\Delta x})^2 & \textit{else} \end{cases}$$

From that, we see that first that $max|H - R| = \frac{9}{52}$ and second that

$$TV(R) = TV(H) + \frac{9}{52}$$

This approximation never converge, neither in the L^∞ norm nor in the BV norm. To illustrate the difficulty of using a non adaptive stencil, we have compared several conservative finite-volume type schemes on the equation

$$u_t + u_x = 0. \tag{9}$$

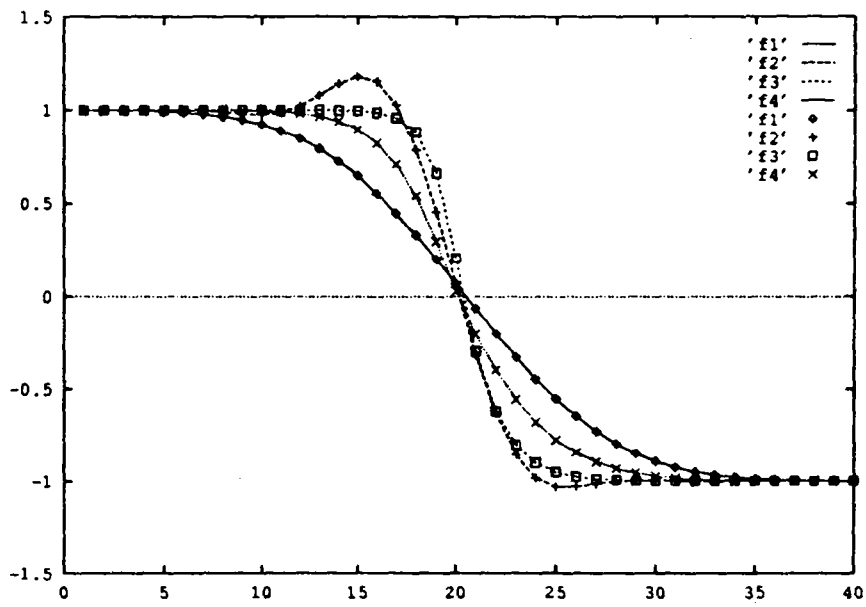

Figure 1: Zoom of the solution of $u_t + u_x = 0$ for several conservative schemes.$\diamond$: first order, = second order MUSCL + fixed stencil, $\times$ second order ENO, $\square$ third order ENO

At the initial time, $u(x, t = 0)$ is a Heaviside function. The results are displayed on Figure 1. The CFL number is set to 0.5 here. The symbol $\diamond$ correspond to a first order upwind scheme. The symbol + correspond to a second order upwind MUSCL like scheme with the fixed stencil x_{i-1}, x_i, x_{i+1}. The symbols $\times$ and $\square$ correspond to ENO schemes, the second order one is $\times$ and the third order one is $\square$. Note that we have used the Runge Kutta time steppings of paragraph 3. From this, it is clear that the second order scheme with a fixed stencil has a problem. If, instead of the linear equation (9), we would have integrated the Burgers equation with the same (stationary) data, the results would have been even worse.

They indicate that one has to give up with the idea of a fixed stencil to reconstruct possibly discontinuous functions. The idea of adaptive stencils has been introduced by Harten et al. [7, 8, 9]. In the next two paragraphs, we introduce their method, and show its limit when one wants to extend it to higher dimensions.

4.2 An Essentially non oscillatory Lagrange interpolation

The classical ENO reconstruction methods are constructed from two well known properties or the Lagrange interpolation of any function u : *consider an increasing subdivision of* $\mathbb{R}$, (y_i), *and* P *a polynomial of degree* r *such that :*

$$P(x_l) = u(y_l) \qquad m \leq l \leq m + r - 1$$

Then

1. *if* u *admits* $n > r$ *continuous derivatives on* $[y_m, y_{m+r-1}]$ *then for any* $x \in [y_m, y_{m+r-1}]$,

$$|P^{(k)}(x) - u^{(k)}(x)| \leq C \max_{m \leq l \leq m+r-2} |y_l - y_{l+1}|^{r-k+1}$$

2. *if the k-th derivative of* u, $k < r$, *admits a jump* $[u^{(k)}]$ *in* $x_0 \in]y_m, y_{m+r-1}[$, *then* a_m, $r \geq m > k$, *the m-th coefficient of* P *in its Taylor development around* x_0 *behave like* $\max_{m \leq l \leq m+r-1} |y_l - y_{l+1}|^{-r+m}$

These two results explains that if if u is smooth then the coefficients of P remains *bounded* when the mesh size decrease but *blow up* if one of the derivative of u of order smaller than the degree of P admits a jump.

From these two remarks, one may construct the following essentially non oscillatory Lagrange reconstruction in a neighborhood of a mesh point y_i. The idea is to construct an "adaptive" stencil $\mathcal{S}_i^k$ the points of which are used to compute the Lagrange interpolation P_i^k, where P_i^k is a polynomial of degree k.

First, we recall that the divided differences table can easily be recursively constructed :

$$\text{k} = 0 \quad [y_i]u = u(y_i)$$

$$\text{k} > 0 \quad [y_i, y_{i+1}, \cdots, y_{i+k-1}, y_{i+k}]u = \frac{[y_{i+1}, \cdots, y_{i+k}]u - [y_i, y_{i+1}, \cdots, y_{i+k-1}]u}{y_{i+k} - y_i}$$

Algorithm :

1. Start with $\mathcal{S}_i^0 = \{y_i\}$

2. for $l \leq k$, consider $\mathcal{S}_i^{l-1} = \{y_{j_0} < \ldots < y_{j_0+l-1}\}$ the stencil for P_i^{l-1}. Compute the divided differences

$$[y_{j_0-1}, y_{j_0}, \cdots, y_{j_0+l-1}]u \text{ and } [y_{j_0}, \cdots, y_{j_0+l-1}, y_{j_0+l}]u.$$

- if $|[y_{j_0-1}, y_{j_0}, \cdots, y_{j_0+l-1}]u| < |[y_{j_0}, \cdots, y_{j_0+l-1}, y_{j_0+l}]u|$ then $\mathcal{S}_i^l = \mathcal{S}_i^{l-1} \bigcup \{y_{j_0-1}\}$,
- else, $\mathcal{S}_i^l = \mathcal{S}_i^{l-1} \bigcup \{y_{j_0+l+1}\}$.

End algorithm

When one applies it to the Heaviside function, one gets

$$R(x) = \begin{cases} 1 & \text{if } x < \frac{\Delta x}{2} \\ -1 & \text{if } x > \frac{\Delta x}{2} \end{cases}$$

It is possible to see that if the function u is smooth, say of class larger than k the degree of the reconstruction, then the derivative of $u - R$ satisfy :

$$max|u^{(l)} - R^{(l)}| \leq Ch^{k+1}$$

where C is a constant that depends on the mesh and u and

$$TV(R) \leq TV(u) + O(h^k).$$

4.3 Application to finite volume schemes

In finite volume schemes, the unknowns are not known at nodes but only mean values on control volumes are given. There are two ways of using the above ENO Lagrange reconstruction in order to get an ENO reconstruction : the so–called *reconstruction via primitive functions* and *reconstruction via deconvolution.*

Reconstruction via primitive functions Let us consider a mesh (x_i) and a real valued function u which averages u_i on the control volumes $[x_{i-1/2}, x_{i+1/2}]$ are given. It is possible to know the values of the primitive W of u defined by

$$W(x) = \int_{x_{1/2}}^{x} u(t)dt$$

at the nodes $x_{i+1/2}$ because

$$W(x_i) = \int_{x_{1/2}}^{x_{i+1/2}} u(t)dt = \sum_{j=0}^{j=i} (x_{i+1/2} - x_{i-1/2})u_i.$$

One constructs a local ENO Lagrange reconstruction of W up to order $k+1$, say P_i^{k+1} of W on the interval $]x_{i-1/2}, x_{i+1/2}[$. Note that the nodes y_i are the $x_{i+1/2}$'s. We then define $R(u,k)$ the reconstruction of u defined on $]x_{i-1/2}, x_{i+1/2}[$ by polynomials of degree k :

$$R(u,k) = \frac{dP_i^{k+1}}{dx} \quad \text{on }]x_{i-1/2}, x_{i+1/2}[.$$

It is clear that if u is smooth enough, then property P1 is true. If u admits only *isolated* discontinuities for itself or one of its derivative, property P2 is also true. Last property P3 is a consequence of the construction :

$$\int_{x_{i-1/2}}^{x_{i+1/2}} R(u,k)dx = P_i^{k+1}(x_{i+1/2}) - P_i^{k+1}(x_{i-1/2}) = (x_{i+1/2} - x_{i-1/2})u_i$$

Reconstruction via deconvolution This method can **only** be applied to **regular** meshes. We can even precise this restriction : all the control volumes must be deduced from one another by translation. The idea is to consider the function v defined by :

$$v(x) = \frac{1}{\Delta x}\int_{-\Delta x/2}^{\Delta x/2} u(t+x)dt$$

Since the mesh is regular, then $v(x_i) = u_i$. Moreover, if u is smooth enough, one may consider the Taylor expansion of u to order k around x. Putting this in the integral and after some simple calculations, this gives

$$v(x) = u(x) + \sum_{l=1}^{k} \alpha_l \Delta x^l \frac{d^l u}{dx^l}(x) + O(\Delta x^{k+1}) \tag{10}$$

with

$$\alpha_k = \begin{cases} 0 & \text{if } k \text{ is odd} \\ \dfrac{1}{(k+1)!\,2^k} & \text{else} \end{cases}$$

When one derives (10), one gets, for $1 \le p \le k$:

$$\Delta x^p \frac{d^p v(x)}{dx^p} = \sum_{l=p}^{k} \alpha_l \Delta x^l \frac{d^l u}{dx^l}(x) + O(\Delta x^{k+1}) \tag{11}$$

so that the collection of equations (8-11) gives :

$$\begin{pmatrix} v(x) \\ \vdots \\ \Delta x^k \dfrac{d^k v(x)}{dx^k} \end{pmatrix} = \begin{pmatrix} 1 & 0 & \frac{1}{3!\,2^2} & \cdots & \frac{1}{(k+1)!\,2^k} \\ & 1 & 0 & \frac{1}{3!\,2^2} & \cdots \\ & & \ddots & \ddots & \ddots \\ & & & \ddots & \ddots \\ & & & & \ddots \\ & & & & 1 \end{pmatrix} \begin{pmatrix} u(x) \\ \vdots \\ \Delta x^k \dfrac{d^k v(x)}{dx^k} \end{pmatrix} + O(\Delta x^{k+1}) \tag{12}$$

Now, we insert the ENO Lagrange interpolation of v at order k in a neighbourhood of x_i (namely $]x_{i-1/2}, x_{i+1/2}[$), P_i^k, instead of v in (12), drop the $O(\Delta x^{k+1})$ and solve this triangular system. Notice here that the y_i's are the x_i's We note the solution by $(a_0, \cdots, a_k)^T$ and define $R(u,k)$ in $]x_{i-1/2}, x_{i+1/2}[$ by

$$R(u,k) = \sum_{l=0}^{k} a_l \left(\frac{x - x_i}{\Delta x}\right)^l.$$

It is clear that $R(u,k)$ satisfies P1 and P2. The property P3 is also satisfied because the first line of (12) gives

$$\frac{1}{\Delta x}\int_{x_{i-1/2}}^{x_{i+1/2}} R(u,k)dx = \sum_{l=0}^{k} \alpha_l \frac{a_l}{l!} = v(x_i) = u_i$$

4.4 Possible extension to higher dimensions, weaknesses

The extension of these method to higher dimensions has been carried out, for example by Casper et al. [12], for *regular structured* grids. The outlines of their method are the following. They first assume their mesh is a Cartesian product $\{(x_i, y_j), 1 \leq i \leq N, 1 \leq j \leq M\}$ and they construct control volumes. With the notation $\Delta_k \xi = \xi_{k+1} - \xi_k$, the datas are

$$\overline{\overline{w}}_{ij} = \frac{1}{\Delta_i x\, \Delta_j y}\int_{x_{i-1/2}}^{x_{i+1/2}}\int_{y_{j-1/2}}^{y_{j+1/2}} w(x,y)dx\, dy. \tag{13}$$

For $y_{j-1/2} < y < y_{j+1/2}$, they consider the primitive function $\overline{W}_j(x)$ associated with w defined by :

$$\overline{W}_j(x) = \int_{x_0}^{x} \frac{1}{\Delta_j y}\left[\int_{y_{j-1/2}}^{y_{j+1/2}} w(\xi,y)dy\right] d\xi \tag{14}$$

From (13), they notice that

$$\Delta_i x \overline{\overline{w}}_{ij} = \overline{W}_j(x_{i+1/2}) - \overline{W}_j(x_{i-1/2})$$

so that they can consider the reconstruction via primitive function of at order k of $\overline{W}_j$: $v_j(x) = R(x,w)_j$.

Then, the procedure (14) is performed for any j. Since

$$\frac{d}{dx}\overline{W}_j(x) = \frac{1}{\Delta_j y}\int_{y_j-1/2}^{y_{j+1/2}} w(x,y)dy,$$

$R(x,w)_j$ can be interpreted as a one-dimensional cell average on $[y_{j-1/2}, y_{j+1/2}]$ of some function $v(x,y)$. For a fixed x, one consider the set $\{R(x,w)_j\}$ and a primitive $V(x,y)$ associated to v

$$V(x,y) = \int_{y_0}^{y} v(x,y)dxdy$$

whose pointwise values are known at the interfaces :

$$V(x, y_{j+1/2}) = \sum_{k=j_0}^{j} \Delta_k y \overline{v}_k(x).$$

We can once more apply the same reconstruction via primitive function to v to order k and construct a reconstruction $R^2(x,y,w) = R(y; R(x;\overline{\overline{w}}))$ of w . It is clear that this new reconstruction will have the conservativity, essentially TVD and precision properties : they are directly inherited from the one-dimensional reconstruction properties.

Remark : This reconstruction is a reconstruction by tensor product. The stencil of a reconstruction of order k has $(k+1)^2$ elements (see figure 2).

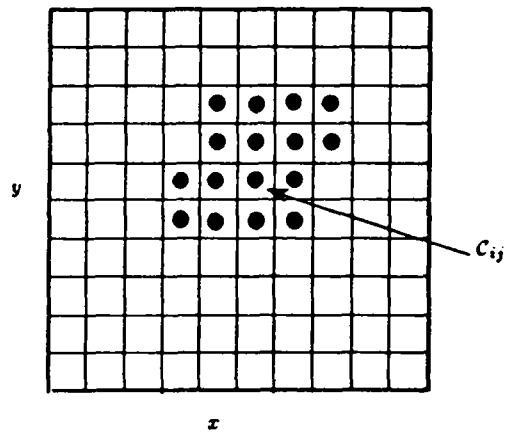

Figure 2: A potential stencil for Casper et al.'s reconstruction, k=3, from [12]

When the mesh is *not* a Cartesian product, one has to assume the existence of a smooth transformation from the physical $x - y$ plane the rectangular $\xi - \nu$ plane :

$$x = x(\xi, \nu) \qquad y = y(\xi, \nu) \tag{15}$$

The Jacobian determinant $J(\xi, \nu)$ should *never* vanish. The control volume C_{ij} of the physical plane are the control volumes

$$\mathcal{D}_{ij} =]\xi_{i-1/2}, \xi_{i+1/2}[\times]\nu_{i-1/2}, \nu_{i+1/2}[$$

mapped by the transformation (15). The averaged values are :

$$\overline{\overline{u}} = \frac{1}{a_{ij}} \int_{\xi_{i-1/2}}^{\xi_{i+1/2}} \int_{\nu_{i-1/2}}^{\nu_{i+1/2}} u(x(\xi, \nu), y(\xi, \nu)) d\xi \, d\nu$$

where a_{ij} is the area of C_{ij}. Then one use the above reconstruction on the $\xi - \nu$ mesh. The reconstruction $\tilde{R}$ is :

$$\tilde{R}(\xi, \nu, \overline{\overline{u}}) = \frac{1}{J(\xi, \nu)} R^2(\xi, \nu, a\overline{\overline{u}})$$

The scaling factors are introduced for $\tilde{R}$ satisfies the conservation property.

From this, it is clear this kind of reconstruction algorithm is very dependent on the structure of the mesh. Generally speaking, these "classical" reconstruction algorithms can be used only in the following context :

- Reconstruction via deconvolution : one needs to interpret the mean value of u as the convolution product of u and the ratio of the characteristic function of a set C and its area, so that the control volumes must be deduced one from another by translation only. In particular, they must have the same area. The scope of the reconstruction via deconvolution is then very limited even if some extension are possible [13].

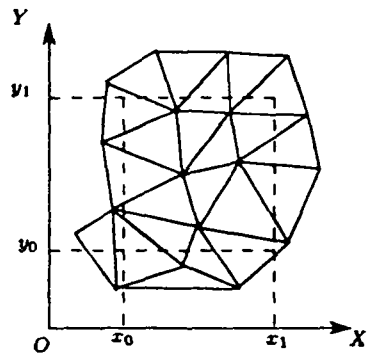

Figure 3: Covering of the rectangle $[x_0, x_1] \times [y_0, y_1]$ by triangular control volumes

- Reconstruction via primitive function : in order to use the same ideas than Casper et al., one needs to gather control volumes by subsets so that their collection is a square. For a reconstruction of degree k, one should be able to gather them by subsets of k^2 sets. This is, in general not possible (see Figure 3 where the control volumes are triangles).

For all these reasons, one needs other algorithms to handle more general geometries. In section 7, we show how this can be done in the general context of unstructured meshes. Before this, we bring out some pathologies of ENO methods and their remedy, then we explain how to implement them on modern vector and parallel machines.

5 ENO and Central Biased ENO Methods

In the computation of discontinuous solutions to hyperbolic systems of conservation laws, the recently developed ENO methods appear to be very useful for reaching high order of spatial accuracy. However, in some cases, the expected order of accuracy may not be numerically obtained. This section is devoted to describing a simple example in which such a failure occur and to presenting several recipes to fix the ENO method by central biasing. Moreover, related algorithms to recover high order of accuracy in smooth regions are described by implementing some hybridizing techniques in which high order ENO and central differences are coupled together.

5.1 A pathological Example

This example will consist in studying the simple linear advection equation :

$$\partial_t u + a\partial_x u = 0, \tag{16}$$

with initial condition

$$u(x,0) = u_0(x) = e^{cx}, \tag{17}$$

in which we choose to take a and c to be non negative coefficients. By the characteristic method, the exact solution is simply

$$u(x,t) = u_0(x - at) = e^{c(x-at)},$$

and therefore, its n^{th} differentiation with respect to x

$$\frac{\partial^n u(x,t)}{\partial x^n} = c^n.u(x,t) \tag{18}$$

stays non negative for all (x,t). Hence, if we want to solve numerically the problem (16) and (17) with some preset boundary conditions that do not matter for our purpose, and implement the ENO method as described in previous section, then it is easy to verify that the order of accuracy is always **two** no matter how high the order of accuracy of the overall method. Of course, this fact contradicts the global theory for which having constructing a high order reconstruction would automatically lead to a high order numerical method. The next paragraphs sketch the main reasons why the interpolation theory combined with cell averages may lead to a wrong conclusion.

To start with, let us come back to the definition of the reconstruction operator and its interpolating stencil that we denote by $R_j(x,\bar{u})$ and $J(j)$ on each cell C_j that we supposed to be uniform of size $h = (x_i - x_{i-1})$ for any index i where x_i are the grid points of the discretized domain. The global reconstruction operator is a piecewise polynomial of degree $p-1$

$$R(x,\bar{u}) = R_j(x,\bar{u}),$$

$\forall x \in C_j$, to get an estimated p^{th} order accurate reconstruction, i.e

$$R(x,\bar{u}) = u(x,.) + O(h^p),$$

for sufficiently smooth u. Of course, the exact solution to above test problem belongs to C^∞ and therefore above conclusion should hold. However, we already numerically check that this is wrong. The main reason comes from the fact that the stencil $J(j)$ for any j is always fully upwinded to the left. In fact, the polynomials are always built using the approximated solutions on cells

$$(x_{j-p+1},...,x_j),$$

because $u(x,t)$ and $\partial_x^n u(x,t)$ are strictly increasing functions. Therefore, the estimated divided differences are all strictly increasing. Consequently, the search for the smoothest part of the solution - which consists in taking the smallest divided differences within the ENO framework - always selects the additional information located to the left of the previous one (refer to the classical 1D ENO algorithm). However, several observations can be pointed out. First, it can observed that the fact of constructing the piecewise polynomial $R(x,\bar{u})$ into the region in which the divided differences of $\bar{u}$ are minimized does not mean that the other regions in which the estimated derivatives of u are larger indicate non smoothness of u. Second, it is well known that for recovering high order of accuracy, some cancellations in the error expansions must occur. Therefore, it seems that above high order ENO method just behaves as a second order upwind method. In fact, we have just realized that the ENO method can degenerate to a linear scheme [1]. Therefore, the non linear process which consists in switching from one additional information to the right and then to the left, and so on, should prevent the ENO method to this troublesome second order degeneracy property in smooth regions. Very recently, A. Harten pointed out (without proof) that the expected order of accuracy

[1] In some cases, depending on the respective signs of a and c, the scheme may become linear with a stencil lying all in a direction oppsite to the upwinding, so that it is linearly unstable. The ENO procedure tends to stabilize the scheme, but the stencil becomes erratic. This leads to a loss of accuracy.

is numerically observed in L^1 norm as long as the ENO stencils are in "averaged" centered. This is equivalent to verifying that the ENO stencils

$$J^{(eno)}(j) = (j - r(j), ..., j + s(j)),$$

where $r(j) + s(j) = p + 1$ are, in average, closed to the centroid point $c(j)$ which are exactly defined for the centered stencils

$$J^{(central)}(j) = (j - n + 1, ..., j + n),$$

where we have set $p = 2n$.

5.2 Study of the Numerical Error

This section is intended to proving why the fully upwinded ENO method is only second order accurate in smooth regions. The test problem defined in previous section (with $c = 0$) is investigated.

Using the reconstruction operator by primitive functions as described in Shu and Osher [10], we devise the reconstruction operator at time $t = 0$:

$$R_j(x, \bar{u}) = D_0 + \sum_{k=1}^{p-1} (x - x_j)^k D_k,$$

where D_k are the divided differences of u in the fully upwinded ENO stencil $(x_{j-p+1}, ..., x_j)$. All calculations done, they reduce to the formulas

$$D_k[x_{j-k}, ..., x_j] = \frac{(1 - e^{-ch})^k}{k! h^k} . e^{cjh}, \tag{19}$$

where we let $x_j = j.h$ for additional simplifications. Next, the reconstructed cell averaged solution on cell C_i, for all $i \in J(j)$ is obtained by the averaging process

$$\bar{u}_i = A(C_i) R(x, \bar{u}) = \sum_{k=0}^{p-1} a_{ik} D_k$$

where $A(C_i)$ is the averaging operator and

$$a_{ik} = \frac{1}{h} \int_{x_i - h/2}^{x_i + h/2} (x - x_j)^k dx = \frac{h^k}{k+1} d_{ijk},$$

in which

$$d_{ijk} = (i - j + 1/2)^{k+1} - (i - j - 1/2)^{k+1}.$$

Hence, on cell C_j, the p^{th} order cell averaged reconstruction simplifies to

$$\bar{u}_j^{(p)} = u_0(x_j) \sum_{k=0}^{p-1} d_{jjk} \frac{(1 - e^{-ch})^k}{(k+1)!}, \tag{20}$$

in which

$$c_{jjk} = \begin{cases} 0 & \text{if } k \text{ is odd,} \\ (\frac{1}{2})^k & \text{otherwise.} \end{cases} \tag{21}$$

Therefore, after expanding out the equation (20), we arrived at

$$\bar{u}_j^{(p)} = u_0(x_j)(c_{jj0} + c_{jj2}\frac{(1-e^{-ch})^2}{3!} + c_{jj4}\frac{(1-e^{-ch})^4}{5!} + ...).$$

Next, by using Taylor expansions of e^{-ch} for small h,

$$e^{-ch} = 1 - ch + \frac{(ch)^2}{2} - \frac{(ch)^3}{3!} + ...,$$

and substituting in above relation, we obtain the simple result :

$$\bar{u}_j^{(p)} = u_0(x_j)(1 + \frac{1}{24}((ch) - \frac{(ch)^2}{2})^2 + O(h^4), \tag{22}$$

where $O(h^4)$ includes all the other terms which are of order h^N, for $N \geq 4$.

To conclude, we compute the exact cell averaged solution at time $t = 0$. By definition, on cell C_j, it reduces to

$$\bar{u}_j^{exact} = \frac{1}{h}\int_{x_j-h/2}^{x_j+h/2} u_0(x)dx = \frac{1}{ch}e^{cjh}(e^{ch/2} - e^{-ch/2}).$$

Factorizing by $e^{ch/2}$, we obtain the relation

$$\bar{u}_j^{exact} = u_0(x_j)e^{ch/2}\frac{1-e^{-ch}}{ch}.$$

Again, by using Taylor expansions and rearranging all terms by increasing powers of h, above relation rewrites :

$$\bar{u}_j^{exact} = u_0(x_j)(1 + \frac{1}{24}(ch)^2 + O(h^4)). \tag{23}$$

Finally, from (22) and (23), we set the formula :

$$\bar{u}_j^{(p)} - \bar{u}_j^{exact} = \frac{1}{24}(ch)^3 u_0(x_j) + O(h^4).$$

This shows that the averaging process destroys the recovery of high order of accuracy of the reconstruction procedure. In fact, if instead, we had averaged the reconstruction operator on the larger cell

$$C_{J(j)} = \cup_{i \in J(j)} C_i,$$

and verified the convergence error of the averaged solution around the centroid of $C_{J(j)}$, then the expected high order of accuracy would have been reached because of two by two cancellations when using Taylor expansions. As seen above, a third order cumulative error is obtained on each cell

which indicates that the fully upwinded ENO method is only second order accurate in L^1 norm. In above calculations, by using the time iteration scheme

$$\bar{u}_j^{n+1} = A(C_j).E(a, \Delta t)R(x, \bar{u}^n),$$

where $E(a, \Delta t)$ is the time evolution operator of Runge-Kutta type, and letting $a = 0$, we proved that $u_h(x_j, t)$ is only second order accurate. However, we can notice that, if only one switch in the search of the ENO stencil from the left to the right is assessed, then a gain of two order of magnitude in the cumulative error is gained, which implies at least fourth order of accuracy.

In the same spirit, other questions of accumulation of errors were studied in [27, 29, 32]. In [27], the selection of the smoothest stencil leads to a scheme which is linearly unstable in the whole interval. It is shown that once the high order derivatives have begun to oscillate and grow, the selection of the stencil became erratic which in turn stabilized the calculations with nevertheless a reduced order of accuracy. In [29], similar loss of accuracy are observed near points at which all derivatives up to a certain order vanish. Finally, in [32], it is demonstrated that such unnecessary loss of accuracy can be avoided by central biasing the selection of the stencil toward a central one in the smooth part of the solution - which is emphasized in above calculations.

5.3 Hybrid ENO Method

In this section, we describe an hybrid reconstruction that allows the selection of a centered stencil in smooth part of the solution and a classical ENO stencil near discontinuities. This algorithm is also described in [15].

To start with, we define two reconstruction operators - one is based on a central stencil $R^{(c)}(x, \bar{u})$ and the other is the classical ENO stencil $R^{(e)}(x, \bar{u})$. The hybrid reconstruction can be symbolically written as

$$R_j(x, \bar{u}) = (1 - \theta_j)R^{(c)}{}_j(x, \bar{u}) + \theta_j R_j^{(e)}(x, \bar{u}),$$

where we defined the automatic switch $\theta_j \in [0, 1]$ so that θ_j is closed to 1 when $J^{(e)}(j)$ contains a singularity and is of order $O(h^{p-r})$ when the solution is smooth in $J^{(c)}(j)$. Here, we have denoted by $J^{(c)}$ and $J^{(e)}$ the centered and ENO stencils, respectively. Moreover, r is the order of the ENO reconstruction ; e.g if $r = 1$, then $R_j^{(e)}(x, \bar{u}) = \bar{u}_j$. From the switch requirements, the formal order of accuracy is preserved even in smooth regions. The switch can be defined as follows. If we denote by

$$\Delta_j^k = \Delta^k \bar{u}_j,$$

the undivided differences of degree k where Δ is the forward differencing operator, then

$$\theta_j^k = \frac{|\sum_{l=0}^{p-k} \alpha_l^k \Delta_l^k|}{\sum_{l=0}^{p-k} |\alpha_l^k||\Delta_l^k| + \varepsilon},$$

where $\alpha_l^k = (-1)^{p-k-l} C_l^{p-k}$ and $C_m^n = \frac{m!}{n!(m-n)!}$ when $m \geq n$, and ε is a small parameter proportional to round off error. This switch satisfies all the previous requirements up to the k^{th} derivative. Two important cases can be investigated :

$$\begin{aligned} |\Delta_l^k| &= \delta_{l,l_0} \\ \Delta_l^k &= (-1)^l |\Delta_l^k|, \end{aligned}$$

where δ_{l,l_0} is the Kroneker δ symbol. The first one corresponds to a step discontinuity in $\partial^k \bar{u}$, whereas the second indicates a discontinuity in $\partial^q \bar{u}$, for $q \leq k$. Therefore, $\theta^k = 1$ for a discontinuity in $\partial^q \bar{u}$ for $k \geq q \geq 0$. Next, in the case $\partial^p \bar{u}$ is smooth, we consider the product $\theta^k D^k$ where

$$D^k = h^k(\partial^k \bar{u}) + O(h^p).$$

Clearly,

$$|\theta^k D^k| = O(\frac{h^p|\partial^p \bar{u}|}{h^k|\partial^k \bar{u}|}).(O(h^k|\partial^k \bar{u}|) + O(h^p)) = O(h^p);$$

note that this remains so even when some of the derivatives of $\partial^k u$ vanish at a point ; i.e

$$\partial^k u = ... = \partial^{k+r-1} u = 0,$$

for some integer r. In this case, the denominator in θ^k is $O(h^{k+r})$, but so is D^k. Thus,

$$\theta^k = O(h^{k-r}) \text{ and } \theta^k D^k = O(h^p).$$

In summary, this method satisfies the following properties :

$$(1 - \theta_j^k).(A(C_j)D_k) = \begin{cases} 0 & k \geq q \geq 0 \\ (A(C_j)D_k) + O(h^q) & k \leq q \leq p \\ (A(C_j)D_k) + O(h^p) & q \geq p \end{cases} \tag{24}$$

where q is the first index for which $\partial_x^{(m)} u$ is discontinuous and D_k is any k^{th} central divided difference of $\bar{u}$. This also implies that $\theta^k = 1$ for all $k \geq q \geq 0$.

5.4 Central Biased ENO Methods

The second type of recipes to recover the formal order of spatial accuracy is based on the fact that any upwinded or centered stencil is welcomed when the solution is smooth enough. To get a more centered ENO stencil, we can modify the selection of the ENO stencil procedure by weighing up the successive derivatives of u. To do so, instead of selecting the smoothest part of the solution by making use of the classical unweighed divided differences

$$\begin{aligned} a^{(s)} &= [x_{k_{min}^{(s-1)}-\frac{1}{2}}, ..., x_{k_{min}^{(s-1)}+s-\frac{1}{2}}]u, \text{ and} \\ b^{(s)} &= [x_{k_{min}^{(s-1)}-\frac{1}{2}-1}, ..., x_{k_{min}^{(s-1)}+s-1-\frac{1}{2}}]u, \end{aligned}$$

where $x_{k_{min}}^{(s-1)}$ is the left point of the ENO stencil at the induction level $s-1$ and $a^{(s)}$, $b^{(s)}$ are the s divided differences computed from the $(s-1)$ ENO stencil with the addition of one data point to the right and to the left, respectively ; we choose to pick the modified ENO stencil

$$\text{if } \delta_1^{(s)} a^{(s)} \geq \delta_2^{(s)} b^{(s)},$$

then $k_{min}^{(s)} = k_{min}^{(s-1)}$, and $k_{min}^{(s)} = k_{min}^{(s-1)} - 1$ otherwise. Here, $\delta_1^{(s)} \geq 1$ and $\delta_2^{(s)} \geq 1$ and $\delta_1^{(s)}$ or $\delta_2^{(s)}$ is identical to 1 if the stencil at level $(s-1)$ is mostly upwinded to the right or to the left, respectively. In the linear advection problem described in section 5.1, we will take $\delta_2^{(s)} = 1$ and $\delta_1^{(s)} = C$ for some non negative constant C. Generally, this constant is chosen in the range 2 to 10. Some numerical tests are presented in [32]. Note that if $\partial^k u$ is discontinuous, then the smoothest part of the solution is still taken since then one of the two undivided difference has a jump discontinuity of the order $O(1/h)$.

5.5 Hybridizing ENO and Central Differences

The last type of hybrid methods that we introduce in this lecture is based on the coupling of ENO methods with more basic central difference approximations. In fact, as seen before, if the solution is smooth, then a centered stencil leads to a non oscillatory scheme. The idea is to implement a centered approximation for the flux functions as much as possible (refer to [30]).

In [30], high order $2p^{th}$ central flux approximations are defined as follows :

- Second Order: $(p = 1)$

$$f_{j+1/2} = \frac{f(u_{j+1}) + f(u_j)}{2}, \tag{25}$$

- Fourth Order: $(p = 2)$

$$f_{j+1/2} = \frac{7}{12}(f(u_{j+1}) + f(u_j)) - \frac{1}{12}(f(u_{j+2} + f(u_{j-1})), \tag{26}$$

- Higher Order $\forall p$: It is a simple matter, using Richardson's extrapolation to construct and obtain arbitrary high order accurate centered difference methods

$$\begin{aligned} f_{j+1/2} &= \sum_{i=-p+1}^{p} \beta_i f(u_{j+i}), \\ \text{where } \beta_{-i+1} &= \beta_i \text{ for } i = -p+1, ..., p-1, \\ \text{and } \sum_{i=-p+1}^{p} \beta_i &= 1. \end{aligned}$$

The hybridization consists then in applying the following algorithm :

- FOR $i = 1, m$ DO

  1. Approximate the partial differential equation such as (16) using above high order centered differences.
  2. IF the updated numerical solution has spurious oscillations **Then** we correct it by recomputing it using ENO fluxes.

- END DO.

At each time, an oscillation is detected at a point, the ENO fluxes are computed for updating the numerical solution in an extended region in order to avoid low frequency oscillations. Moreover, a non linear detector for detecting rapid changes in the gradient of the numerical solution from one time step to the other is implemented

$$\Delta_{\pm} u_j^n \Delta_{\pm} u_j^{n+1} \leq (\Delta x)^2 \Big(-1 + \cos\alpha \sqrt{1 + \Big(\frac{\Delta_{\pm} u_j^n}{\Delta x}\Big)^2} \sqrt{1 + \Big(\frac{\Delta_{\pm} u_j^{n+1}}{\Delta x}\Big)^2}\Big),$$

where α is a preset angle and $\Delta_{\pm} u_j^{n+1} = \pm(u_{j\pm1} - u_j)$ are the forward and backward differences. When the above test is positive, then one switches to ENO.

6 Vectorized and Parallelized ENO Methods

First of all, it is easy to derive a fully vectorized ENO algorithm

- 1.) Compute the undivided differences of u_h as follows: let $\phi(j,0) = u_j$, for $j = 1,...,NV$ and construct the undivided difference table $\phi(j,k+1) = \phi(j+1,k) - \phi(j,k)$, for $k = 1,...,p$ and $j = 1,...,N$, where N is the number of grid points.
- 2.) For $k = 1,...,p$, at each grid point x_j, evaluate the ENO interpolating polynomials $P^{(k)}_{j+\frac{1}{2}}(x)$ as follows : first compute the ENO stencil and start with $k^{(1)}_{min} = j$. Then, define the successive ENO stencils by this procedure : if $(|\phi(k^{(k)}_{min},k)| \geq |\phi(k^{(k)}_{min},k)|$ then $k^{(k+1)}_{min} = k^{(k)}_{min} - 1$.
- 3.) Compute the fluxes $F_{j\pm 1/2} = \frac{1}{\Delta x}\sum_{k=1}^{m} C(k^{(k)}_{min} - j, k)\phi(k^{(k)}_{min},k)$, where C is a small matrix with coefficients $C(n,p) = \frac{1}{p!}\sum_{s=n}^{n+p-1}\sum_{l=n,l\neq s}^{n+p-1}(-l)$.

Notice that the matrix C is independent of u_h and thus can be computed once and then stored. Moreover, this algorithm can be extended to several dimensions by dimension by dimension techniques. The overall algorithm is convenient for vectorization purpose since the loop in k is outer whereas the loops over the grid points in any space dimensions are the inner ones. The interior numerical test for the selection of the stencil deteriorates the maximum performance by a reduction factor of approximately 10 to 20 %.

For parallelizing the ENO algorithm, we investigate two different approaches. The first one is closely related to the domain decomposition in which the domain is partitioned into several blocks of approximately identical sizes. In that case, the fluxes or the reconstructions are computed on each processor on a given subdomain. To accomplish all the calculations, the reconstruction procedure needs $(p-1)$ data points which have to be stored. Therefore, an overlapping set of $p-1$ points in each direction of the subdomains must be taken. For example, if the subdomain has size $(0,n1)\times(0,n2)$ for some integers $(n1,n2)$, then all data points in the square $(-p+1,-p+1),...,(n1+p-1,n2+p-1)$ are necessary within the reconstruction procedure.

The last algorithm that we present describes the optimal procedure for implementing the ENO method on a multiple processor parallel computer such as a connection machine. The following 1D example is written in CM Fortran.

% the divided differences are stored in the array $d(0..p-1,j)$, where $d(0,j) = u_j$.

1. $sum = d(0,:)$
2. $A = 0$
3. $A(0,:) = 1$
4. $inc = 0$
5. DO $k = 1,p$
   (a) $d1 = 0$
   (b) $d2 = 0$
   (c) $temp(0,:) = d(k,:)$

(d) DO $k1 = 0, k-1$

i. $d1 = d1 + A(k1,:) * temp(k1,:)$

ii. $temp(k1+1,:) = cshift(temp(k1,:), 2, -1)$

iii. $d2 = d2 + a(k1,:)temp(k1+1,:)$

(e) END DO

(f) WHERE $(d2.ge.d1)$

(g) $inc = inc + 1$

(h) ENDWHERE

(i) DO $k1 = 0, k$

i. WHERE $(inc.eq.k1)$

ii. A(k1,:)=1

iii. ELSE WHERE

iv. A(k1,:)=0

v. END WHERE

(j) END DO

(k) % Update the polynomial reconstruction.

(l) DO $k1 = 0, k$

i. sum=sum+temp(k1,:) * A(k1,:) * coef(k1)

(m) END DO

In this algorithm, the main difficulty resides in avoiding communications between two nodes. This is why we use the intermediate matrices *inc* and A to hide unnecessary values of the divided differences. Moreover, this algorithm becomes rapidly costly because of many cshift operations. For a p^{th} order reconstruction, $(p-1)(p-2)/2 = 0 + 1 + ... + p - 1$ shifts are necessary in order to avoid intermediate indexing in the ENO selection process. Here, it is replaced by the A matrix which is all zero at each level $k1$ except one coefficient which is identical to one for selecting the appropriate ENO stencil.

7 The reconstruction problem on unstructured meshes

7.1 Preliminaries

In the sequel, the symbol $\mathbb{R}_n[X,Y]$ denotes the set of polynomials P in the variables X and Y of total degree less or equal to n :

$$P(X,Y) = \sum_{l=1}^{n} \sum_{i+j=l} a_{ij} X^i Y^j$$

The set $\mathbb{R}_n[X,Y]$ is a vector space of dimension $N(n) = \frac{(n+1)(n+2)}{2}$, a basis of which is the set of monomials

$$\left\{(X-x_0)^i (Y-y_0)^j\right\}_{i+j \leq n}$$

where (x_0, y_0) is any point of $\mathbb{R}^2$. The total degree of P does not depend on the choice of (x_0, y_0). As we will show it latter, this kind of basis is not the best suited for practical calculations.

Let $\mathcal{M}$ be a mesh of the finite element type. Associated with this mesh, we also consider a triangulation $\mathcal{T}$. We may consider several kind of control volumes, for example the triangles of $\mathcal{T}$ themselves or the dual mesh (see Figure 7). They are constructed as follows : for each point M_i, the control volume is obtained by connecting the midpoints of the segments adjacent to it and the center of gravity of the triangles it is a vertex of. Let us denote by $\{C_i\}$ the set of control volume. We only require the following properties :

- For any $i \neq j$, $C_i \bigcap C_j$ is of empty interior,
- C_i is connected,
- There is an algebraic dependency of the C_i's in term of the points of $\mathcal{M}$. This is true for the two above examples.
- The boundary of C_i is a locally regular curve. This is also true for the two above examples.

We consider the following problem (problem $\mathcal{P}$ or approximation in the mean for short) :

Let u be a regular enough function (say in L^1). Given N and n two integer numbers, a set of control volumes $\mathcal{S} = \{C_{i_l}\}_{1 \leq l \leq N}$, find a element $P \in \mathbb{R}_n[X, Y]$ such that for $1 \leq l \leq N$,

$$< u >_{C_{i_l}} \stackrel{def}{=} \frac{\int_{C_{i_l}} u \, dx}{area(C_{i_l})} =< P >_{C_{i_l}} \tag{27}$$

For that problem to have a unique solution, one must fulfill two conditions :

- $N = \frac{(n+1)(n+2)}{2} = N(n)$
- the following Vandermonde type matrix must be non singular :

$$\mathcal{V} = \left[< X^i Y^j >_{C_{i_l}}\right]_{\substack{i+j \leq n \\ 1 \leq l \leq N}} =$$

$$\begin{bmatrix} 1 & < X >_{C_{i_1}} & < Y >_{C_{i_1}} & \dots & < X^n >_{C_{i_1}} & < X^{n-1}Y >_{C_{i_1}} & \dots & < X^n >_{C_{i_1}} \\ \vdots & \vdots & \vdots & \vdots & \vdots & \vdots & \vdots & \vdots \\ 1 & < X >_{C_{i_N}} & < Y >_{C_{i_N}} & \dots & < X^n >_{C_{i_N}} & < X^{n-1}Y >_{C_{i_N}} & \dots & < X^n >_{C_{i_N}} \end{bmatrix} \tag{28}$$

If $\Delta_{\mathcal{S}} = \det \mathcal{V} \neq 0$, then we will often say that this stencil is admissible. In that case, there is a unique solution to problem $\mathcal{P}$ that will be denoted by P_u.

A similar problem was first consider by Barth et al. [17] for smooth functions, then by Harten et al. [15], Vankeirsblick et al. [16, 28] and Abgrall [13]. In the four first references [17, 15, 16, 28], the authors consider overdetermined systems for two reasons : first, the problem $\mathcal{P}$ has not always a unique solution, second they claim that the condition number of the overdetermined system is better than that of problem $\mathcal{P}$. In [13], the same approach as here was adopted. To support that

choice, we must notice, as it is explained in remark 1, that (28) is generally not singular. Second, the condition number of the linear system mainly depends on the basis used for the polynomial expansion, as it is shown in section 7.4. For these two reasons, we have preferred this approach which has the advantage of simplifying the coding of the global scheme. We will come back to this problem, and related ones, in the section 7.7.

Remarks :

1. We do not know if the admissibility condition admits a geometric interpretation (except for $n = 1$). We do not even know whether there is a systematic way of constructing admissible stencils, as it is the case for the Lagrange interpolation [18]. Nevertheless, one may say that in general, any stencil is admissible : one may consider the equation $\Delta_{\mathcal{S}} = 0$ as an algebraic surface in $\mathbb{R}^{2\times k}$ for some integer k [2]. This surface is then of empty interior, from a topological point of view, so that if $\mathcal{S}$ is not admissible, one only have to change slightly the elements of $\mathcal{S}$ for it to become admissible. Nevertheless, the condition number of the linear system may be very bad. We will discuss that point in section 7.4.

2. This admissibility condition is independent of the basis chosen for expanding the polynomial P.

7.2 Some general results about the approximation in the mean

In this section, we give two results on the reconstruction in the mean approximate a given function u when it is smooth or not. They generalize well known properties on the Lagrange interpolation of 1D real valued functions that have been used as a corner stone by Harten and his coauthors to design an essentially non oscillatory reconstruction. We have to emphasis that the reconstruction in the mean in *not* directly related to the Lagrange one. Throughout this section, if $\mathcal{S}^{(n)}$ is an admissible stencil for degree n, the symbol $K(\mathcal{S}^{(n)})$ denotes the convex hull of the union of the elements of $\mathcal{S}^{(n)}$.

7.2.1 Case of a smooth function

In [13], we have shown the following result. Its proof follows easily from Ciarlet & Raviart's proof [22] on Lagrange and Hermite interpolation :

Theoreme 7.1 *Let $\mathcal{S}$ be an admissible (for degree n) stencil of $\mathbb{R}^2$, let h and ρ be respectively the diameter of $K(\mathcal{S})$ and the supremum of the diameters of the circles contained in $K(\mathcal{S})$. Let u be a function that admits everywhere in $K(\mathcal{S})$ a $n+1^{th}$ derivative $D^{n+1}u$ with*

$$M_{n+1} = sup\{||D^{n+1}u(x)||; x \in K(\mathcal{S})\} < +\infty$$

If P_u is the solution of problem $\mathcal{P}$, then for any integer m, $0 \leq m \leq n$,

$$sup\{||D^m u(x) - D^m P_u(x)||; x \in K(\mathcal{S})\} \leq C M_{n+1} \frac{h^{n+1}}{\rho^m}$$

[2] because we have assumed an algebraic dependency of the control volumes in terms of the points of $\mathcal{M}$

for some constant $C = C(m, n, \mathcal{S})$. Moreover, if $\mathcal{S}'$ is obtained from $\mathcal{S}$ by an affine transformation (i.e there exists $x_0 \in \mathbb{R}^2$ and A invertible matrix such that

$$C'_k \in \mathcal{S}' \text{ iff there exists } C_k \in \mathcal{S} \text{ such that } C'_k = A\, C_k + x_0 \ )$$

then

$$C(n, m, \mathcal{S}) = C(n, m, \mathcal{S}')$$

This result basically expresses that if the stencil $\mathcal{S}$ is not too flat, *i.e.* the ratio h/ρ is not too big, then P_u will be a good approximation of u. Let us turn now to the case of unsmooth functions.

7.3 Case of an unsmooth function

We only discuss the case of piecewise smooth functions. This is large enough for our purpose. To do the analysis, we have to introduce the following property which prevents from geometrical degeneration :

Property 7.2 *Let us give $\epsilon > 0$. The admissible stencil $\mathcal{S}^{(n)}$ belongs to $\mathcal{P}^n_\epsilon$ if and only if : for any vector U which component are either 0 or 1 such that both values are represented, let P the n^{th} order polynomial defined by*

$$< P >_{C_{i_j}} = U_j, \quad \text{for all } C_{i_j} \in \mathcal{S}^{(n)}.$$

The sum of the absolute value of the n-th order coefficients of P is greater or equal to ϵ, that is

$$\sum_{l=N(n-1)+1}^{N(n)} \left| \frac{det(R_0 \cdots R_{N(n-1)} \cdots \widehat{R}_l \cdots R_{N(n)})}{det(R_0 \cdots R_{N(n-1)} \cdots R_l \cdots R_{N(n)})} \right| \geq \epsilon. \tag{29}$$

In (29), we have adopted the lexicographic ordering for the monomials $\{X^i Y^j\}_{i+j \leq n}$, so that R_k stands for the k^{th} column of the determinant (28) and $\widehat{R_l} = U$.

Then we can prove [13] the following theorem that describes the asymptotic behavior of the leading coefficients of the approximation in the mean of a piecewise smooth function :

Theoreme 7.3 *Let ϵ be a positive real number and $\mathcal{S}$ an admissible stencil for degree n such that there exists an affine transformation $\mathcal{A}$ as in theorem 7.1 for which $\mathcal{A}(\mathcal{S}) \in \mathcal{P}^n_\epsilon$ Let (x_0, y_0) be any point of the set $K(\mathcal{S})$ and u a real valued function defined on a open subset Ω of $\mathbb{R}^2$ containing $K(\mathcal{S})$. We assume that u is C^{p-1}, $p < n$, in Ω and, except on a locally C^1 curve, admits a continuous and bounded p^{th} derivative with a jump $[D^p u]$, $|[D^p u]| > M_p > 0$. Then, the highest degree coefficients of the Taylor expansion of P_u satisfies*

$$\sum_{i+j=n} |a_{ij}| \geq C(n, p, \epsilon) \frac{M_p}{h^{n-p}} \tag{30}$$

where $C(n, p, \epsilon)$ is a constant independent of $\mathcal{S}$ and invariant by affine transformation.

7.4 Study of the linear problem to solve for the reconstruction

In this section, we intend to study the numerical system to solve to get P_u from the data. We will consider two kinds of expansion of P_u :

1. the "natural" expansion : for any point $(x_0, y_0) \in \mathbb{R}^2$,

$$P_u = \sum_{i+j \leq n} a_{ij}(X - x_0)^i (Y - y_0)^j \tag{31}$$

2. an expansion using "barycentric" coordinate that we describe now : let $\mathcal{S}^{(n)} = \left\{C_1, C_2, C_3, \ldots, C_{N(n)}\right\}$ be an admissible stencil. Hence, at least one subset of three elements of $\mathcal{S}^{(n)}$ is an admissible stencil for $n = 1$.We may assume that the set $\{C_1, C_2, C_3\}$ is admissible. We consider the three polynomials Λ_i of degree 1 defined by :

$$< \Lambda_i >_{C_j} = \delta_i^j, \quad 1 \leq i \leq 3, \quad 1 \leq j \leq 3. \tag{32}$$

The symbol δ_i^j is the Kronecker symbol. Clearly, we have $\Lambda_1 + \Lambda_2 + \Lambda_3 = 1$. These polynomials are the barycentric coordinates of the triangle constructed on the gravity centers of C_1, C_2, and C_3. In order to get expansion (31), a strategy may be to look first for the expansion of the polynomial P_u in terms of power of Λ_2 and Λ_3 :

$$P = \sum_{i+j \leq n} a_{ij} \Lambda_2^i \Lambda_3^j \tag{33}$$

and then to get the Taylor expansion of P_u around the center of gravity of C_1 from (33) (the theorems 7.1 and 7.3 give the behavior of the leading coefficients of P_u whatever the point chosen in the convex hull of $\mathcal{S}$).

In order to get the expansions (31) or (33), one has to solve linear $N(n) \times N(n)$ systems :

$$\mathcal{B}(a_{00} \cdots a_{0n})^T = (< u >_{C_{i_1}} \cdots < u >_{C_{i_{N(n)}}})^T \tag{34}$$

where the matrix $\mathcal{B}$ is obtained by taking the average of $(X - x_0)^i (Y - y_0)^j$ for (31) and $\Lambda_2^i \Lambda_3^j$ for (33). Let us now study the properties of these linear systems.

7.4.1 Case of expansion (30)

A very easy consequence of the inequality (30) is that :

Proposition 7.4 *Let us assume that the conditions of theorem 7.3 holds, and let h be the supremum of the diameters of the spheres containing $K(\mathcal{S}^{(n)})$. Then the condition number of system (34) is at least $O(h^{-n})$ for h small enough.*

Proof : For the sake of simplicity, we consider the following norm on $\mathbb{R}_n[X, Y]$: for $P = \sum_{i+j \leq n} a_{ij}(X - x_0)^i (Y - y_0)^j$, $||P|| = \sum_{i+j \leq n} |a_{ij}|$. On $\mathbb{R}^{N(n)}$, we consider the L^1 norm. Let U be a set of data for the right hand side of (34), and consider the perturbation δU,

$$\delta U = (0 \cdots \epsilon \cdots)^T$$

where ϵ is at the l th position, $l \geq N(n-1)+1$. All the other entries of U are zero. If one considers the function u defined on $\bigcup C_i$ by :

$$x \in C_i, \quad u(x) = \delta U_i,$$

one can apply theorem 7.3. Hence, the perturbation δP has a norm satisfying :

$$||\delta P|| \geq \sum_{i+j=n} |\delta a_{i,j}| \geq C \frac{\epsilon}{h^n}$$

since $||\delta U|| = \epsilon$. This complete the proof. •

This fact is well known for 1D Lagrange interpolation and has motivated the search of more efficient algorithms, such as the Newton algorithm. There exist algorithms that generalizes it [19, 20]. They involve numerous solutions of linear systems, so that we have preferred a more classical approach (see section 7.5), for which the coefficients of the linear systems are obtained from the "barycentric" coordinate expansion (33) as it is explained now.

7.4.2 Case of expansion (32)

In the case of expansion (33), we have the following result :

Proposition 7.5 *If property 7.2 holds for some $\epsilon > 0$, then the condition number of the system (34) for the expansion (33) is bounded above and below by constants independent of h, the supremum of the diameters of the circles containing $K(\mathcal{S}^{(n)})$.*

Proof : The proof is also based on that of theorem 7.3. As in proposition 7.4, the only thing that we have to do is to study the effect on the $a_{i,j}$'s of a perturbation δU. We denote by P the polynomial which averages are defined by δU. The proof can be achieved in two stages :

1. Let B any invertible matrix. Consider the stencil

$$\widehat{\mathcal{S}^{(n)}} = \left\{ B[C_{i,}] + x_0 \right\}_{1 \leq j \leq N(n)}$$

for any x_0. It is clear, from the definition of the Λ_i's that $\widehat{\Lambda}_i(\hat{x}) = \Lambda_i(x)$ if $\hat{x} = Bx + x_0$. Hence, the sum $S(P)$ of the absolute values of the coefficients of P in the basis $\Lambda_2^i(x)\Lambda_3^j(x)$ is the same as that of the development of P in the basis $\widehat{\Lambda}_2^i(\hat{x})\widehat{\Lambda}_3^j(\hat{x})$. This is an homogeneity property.

2. Since the set of stencils defined by property (7.2) is compact, $S(P)$ is bounded below and above, independently of B, hence independently of h :

$$C_1 \geq F \geq C_2(\epsilon, n) > 0.$$

The constant $C_2(\epsilon, n)$ is larger than zero because $\delta U \neq 0$

This achieves the proof •

7.5 The explicit calculation of the reconstruction

From the previous results, the evaluation of the coefficients a_{ij} in (31) is done through those of (33) and hierarchally. For the sake of simplicity, we assume that for any $p \leq n$, the set $\mathcal{S}^{(p)}$ of the $N(p)$ first elements of $\mathcal{S}^{(n)}$ is an admissible for order p. This can be achieved with a suitable numbering of the elements of $\mathcal{S}^{(n)}$. The idea is, instead of looking directly for the coefficients of $P^{(n)}$, to get first those of all of the $P^{(k)}$'s, the reconstruction over $\mathcal{S}^{(k)}$, for $1 \leq k \leq n$ and then to construct those of $P^{(n)}$. In the ENO algorithm described in section 7.6, this involves *no* extra cost and simplifies the evaluation of the a_{ij}'s. This has also the advantage of reducing the size of the linear systems and also to improve their condition number. Assume that $P^{(1)}, \ldots, P^{(p)}$ are known.

We first get the coefficients of $P^{(p+1)} - P^{(p)}$,

$$P^{(p+1)} - P^{(p)} = \sum_{i+j \leq p+1} a'_{ij} \Lambda_2^i \Lambda_3^j$$

by solving the linear system

$$A_{p+1} \begin{pmatrix} \underline{a_1} \\ \underline{a_2} \end{pmatrix} = \begin{pmatrix} A_p & B_{p\,p+1} \\ C_{p\,p+1} & D_{p\,p+1} \end{pmatrix} \begin{pmatrix} \underline{a_1} \\ \underline{a_2} \end{pmatrix} = \begin{pmatrix} \underline{u_1} \\ \underline{u_2} \end{pmatrix} \tag{35}$$

In equation (35), $\underline{a_1}$ (respectively $\underline{a_2}$) stands for the coefficients $\{a_{ij}\}_{i+j \leq p}$ (resp. $\{a_{ij}\}_{i+j=p+1}$). The block matrices A_p, $B_{p\,p+1}$, $C_{p\,p+1}$ and $D_{p\,p+1}$ are defined according to this decomposition. In particular, we notice from the hypothesis that A_p is invertible.

From the conservativity property, we get $\underline{u_1} = 0$, so that the system (35) can be splitted :

$$\begin{aligned} \underline{a_1} &= -A_p^{-1} B_{p\,p+1} \underline{a_2} \\ \left[-C_{p\,p+1} A_p^{-1} B_{p\,p+1} + D_{p\,p+1}\right] \underline{a_2} &= \underline{u_2} \end{aligned} \tag{36}$$

Since $\mathcal{S}^{(p+1)}$ is admissible, $E_p = \left[-C_{p\,p+1} A_p^{-1} B_{p\,p+1} + D_{p\,p+1}\right]$ is also invertible, so that one can get $\underline{a_2}$, then $\underline{a_1}$ and last the coefficients of $P^{(p+1)}$.

Simple manipulations show that

$$A_{p+1}^{-1} = \begin{pmatrix} A_p^{-1} B_{p\,p+1} E_p^{-1} C_{p\,p+1} A_p^{-1} + A_p^{-1} & -A_p^{-1} B_{p\,p+1} E_p^{-1} \\ -E_p^{-1} C_{p\,p+1} A_p^{-1} & E_p^{-1} \end{pmatrix}$$

so that one can quite easily look for the next step. In our case, since the total degree of the reconstruction is less or equal to 4, at most two stages of that method is needed.

Last, one must notice that the condition number of that method is always better that that of the original one because it depends only on that of parts of the original system.

7.6 The E.N.O reconstruction

In [13], we have found that only a few number of stencils was indeed necessary to achieve an essentially non-oscillatory reconstruction of a piecewise smooth function. This set has to be as isotropic as possible. Moreover, the ENO reconstruction was found to achieve the expected order of accuracy for smooth functions, even on very irregular meshes. In what follows, a_{ij} always stands for any of the coefficients of the reconstruction P in the natural basis, $\{(X - x_0)^i (Y - y_0)^j\}$.

Let us describe our procedure up to fourth order :

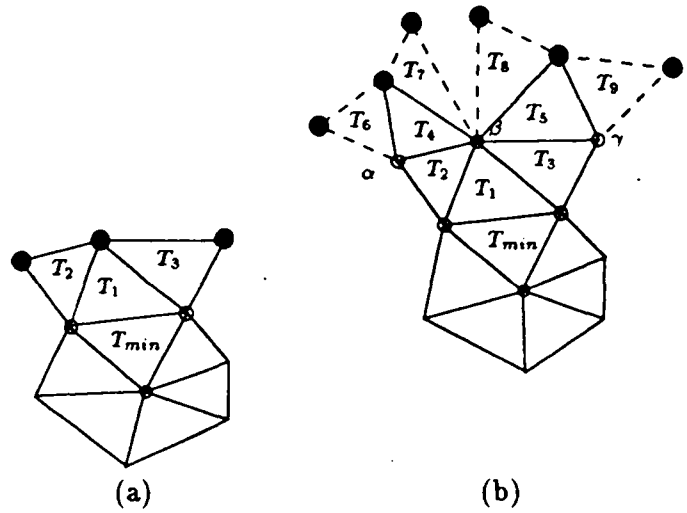

Figure 4: Stencils for third and fourth order reconstruction

1. Let us start from a given cell, C_0 assigned to a point of $\mathcal{M}$, say (x_0, y_0).

2. Consider all the triangles having (x_0, y_0) as a vertex, and choose the one, say T_{min}, that minimize
$$\sum_{i+j=1} |a_{ij}|.$$
Here, $\mathcal{S}^{(1)}$ is the set of control volumes affected to the vertices of T_{min}, (see Figure 4-a). For a regular unstructured mesh, there are about six possible triangles.

3. Consider T_{min}. For any of its three edges, consider the three triangles, T_1, T_2, T_3 as in Figure 4-a. There are three possible configurations. We choose the one that minimize the sum
$$\sum_{i+j=2} |a_{ij}|.$$

4. Consider, as in Figure 4-b, the configuration for third order. It is obtained as follows : for a stencil $\mathcal{S}^{(2)}$ made of the control volumes associated to the vertices of $\{T_{min}, T_1, T_2, T_3\}$, one may consider its "edges" made of the external sides of $\{T_2, T_3\}$, $\{T_2, T_{min}\}$, $\{T_{min}, T_3\}$. Consider one of them, say $\{T_2, T_3\}$, and the vertices α, β and γ. Since the triangulation is conformal, there exist a triangle $T_4 \neq T_2$ on the other side of $[\alpha, \beta]$. Consider T_6 for $[\beta, \gamma]$. Then, for the same reasons, one can construct T_6, T_7, T_8 and T_9. The stencils for fourth order reconstruction are the union of $\mathcal{S}^{(2)}$ and the control volumes associated to the additional vertices of either $\{T_4, T_5, T_6, T_7\}$ or $\{T_4, T_5, T_9, T_8\}$ or $\{T_4, T_5, T_7, T_8\}$. For a stencil $\mathcal{S}^{(2)}$, there are at most 12 stencils for fourth order reconstruction.

The situations seems to be become more and more complicated as the degree increases. Nevertheless, there is a very easy way to simplify it, so that at each level only three stencils for $n+1$th order have to be considered from a n-th order one, as we did from second order to third order.

Let us give a mesh $\mathcal{M}$, we want to derive a $k+1$ th order reconstruction method. The idea is to work with the control volumes defined for a mesh $\mathcal{M}'$ the points and the triangulation of which are constructed from those of $\mathcal{M}$ by adding, for each triangle of $\mathcal{M}$, the points and the triangles associated to a the P_k Lagrange interpolation [21].

7.7 Comparison with different authors

Several authors have studied the problem of the reconstruction of unsmooth function on unstructured grid. We may cite P. Vankeirsbilck [28, 16] and A. Harten in collaboration with S.K. Chakravarthy [15]. In this subsection, we would like to compare our method and theirs.

7.7.1 Evaluation of the reconstruction

Here, we assume that a stencil $\mathcal{S}$ is given for the cell C in the vicinity of which we want to reconstruct some function u represented by its averages on cells with a polynomial P of degree k. This polynomial should fit the data according to two properties :

- The mean of P on C is that of u,
- The reconstruction procedure must represent the polynomial functions of degree $\leq k$ exactly over the whole cell C.

P. Vankersbilck uses three algorithms to represent such a polynomial. In the first one, directly inspired of Barth's [17], P is the linear combination of the constant polynomial ($P=1$) and zero mean value polynomials :

$$F_{ij}(x,y) = (x-x_0)^i(y-y_0)^j - \frac{\int_C (x-x_0)^i(y-y_0)^j dxdy}{\text{Area}(C)}.$$

The constraints are that all the polynomial functions of degree $\leq k$ are exactly represented, so that at least $(k+1)(k+2)/2$ cells are needed. In practice, more cells are given (see further subsection), mainly to improve the condition number of the linear system. This one is solved by a modified Gram-Schmidt algorithm with column pivoting. When the system is overdetermined, the arbitrary constants are obtained by imposing the sum of the square of the coefficients on the F_{ij} basis of the monomials $(X-x_0)^i(Y-y_0)^j$ is minimal on each cells. Vankeirsbilck notes that this algorithm does not guaranty that the average of P on C is that of u so that he modifies it slightly by imposing :

$$P = < u >_C + \sum_{1 \leq i+jk} V_{ij} F_{ij}(x,y).$$

The property on the mean is got by construction. In his last algorithm, the mean value in a cell is affected to its gravity center and a Lagrange polynomial expansion is applied.

In [15], the decomposition of the polynomial function P is done on the standard basis,

$$P(x,y) = \sum_{0 \leq i+j \leq k} a_{ij}(x-x_0)^i(y-y_0)^j$$

and is obtained by imposing the same condition as we do : P should have the same mean as u on all the elements of $\mathcal{S}$. This stencils should have at least $(k+1)(k+2)/2$ cells but in practice, the

authors claims that it is better to increase the number of element to improve the condition number of the system.

In these two examples, the key problem is the condition number of the linear system which solution describes the reconstruction P. The reconstructions of Vankeirsbilck or that of Harten and Chakravarthy use polynomial expansions that are very near or similar to the natural expansion. We have shown above that the condition number of the system become very poor, so that we believe that our choice is better. Moreover, since the control of the condition number is better, less stencils may be used. Last, our choice leads to a rather natural hierarchical algorithm that looks like the Newton algorithm for one-dimensional functions.

7.7.2 Stencil selection

In each case, the stencils contains the cell C_i on which the reconstruction is affected. P. Vankeirsbilck proposes two methods for selecting a stencil :

- Algorithm "Support Selection by Marching" (SSM). It is based on a marching procedure where the marching is done on a criteria such that both the first order gradient and its relative variation on the whole stencil are minimal. One first starts from the cell C and add two neighbouring cells. With these three cells, it is possible to compute, in general, a gradient. The first stencil is the set of three cells that minimizes this gradient. Once this is done, we add cell by cell to this first stencil, but enough to be able to compute a reconstruction of order k ; hence, at least $(k+1)(k+2)/2$ cells. The criterion for selecting or not a stencil is based on the minimization of the linear gradients and their relative variation on the whole stencil. Hence, as this is explained in theorem 7.3, all the informations on the possible jumps of derivative ≥ 1 are lost. In our opinion, this is the main reason why the author tells this method should be used with care [28].

- Algorithm "Support Selection for Global norm mimization" (SSG). This one is also used by Harten et al [15] and this time is base on the minimization of the global norm :

$$\sum_{i+j\geq 0}^{i+j\leq k} \left(\frac{\partial^{i+j} P}{\partial x^i \partial x^j} \right)^2 \tag{37}$$

  so that all derivative are taken. As theorem 7.3 claims it, the criterion is much better. Now, the stencil selection is processed in two step :

  1. One first look to the sector of the plane that give a minimal second order reconstruction ($k = 1$),
  2. then one looks in that sector for the elements of the stencils that minimize (37)(see Figure 5, directly inspired from [28]).

  Overdetermined systems are used in each case.

  The problem of this method may be the following : once a direction has been chosen, one has to stay in that direction. For example, take the 1-D example of Figure 6 as Vankeirsbilck. The cell is located around P, and the algorithm will tend to select point 1 for the first step. Then one has to move in the direction of $\vec{P1}$, contarily to the ENO philosophy. Depending

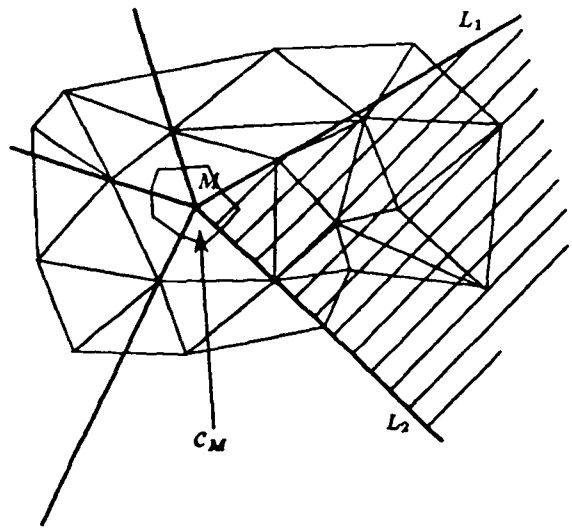

Figure 5: Division by sectors

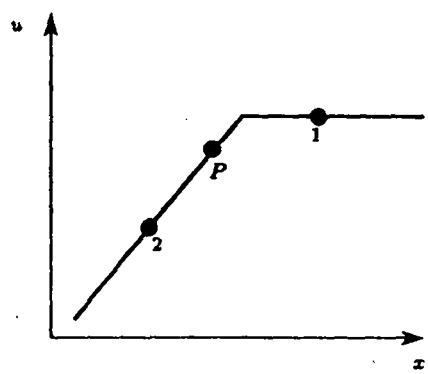

Figure 6: Discontinuous derivative in 1D

on the shape of u and the hights of P, 1 and 2, this method may lead to creating spurious oscillations. On the contrary, our method enable to "come back" if necessary. For a one-dimensional problem, it is similar to the classical 1-D Eno algorithm.

Last these authors have used the concept of central stencils contrarily to us : the selection of the stencil is biased toward the central stencil when u is smooth. This is a good choice in principle. Nevertheless, this concept is left rather vague, to our opinion. Within the Finite Element like framework that is ours, this concept could probably be precised by inspiring oneself of the Galerkin methods [23].

8 Numerical examples

We have performed several tests on the second, third and fourth order E.N.O. interpolation and E.N.O. reconstruction, but we only report the third and fourth order results since they are *a priori* more challenging. In particular, we intend to check numerically that the expected order of accuracy is in fact reached for smooth functions.

In all these examples, we have assumed that the control volumes are of the element of the dual mesh (see Figure 7). The practical calculations of the averages in these control volumes have been performed with a 5-th order quadrature formula [21].

The tests on smooth functions are performed on :

$$u(x,y) = \cos(2\pi(x^2+y^2)).$$

The mesh size h has been measured by choosing the largest segment of the triangulation. All the error estimates have been obtained on irregular meshes as the one presented on Figure 8. These meshes are obtained as random perturbations of regular structured meshes. The set of points that one obtains is triangulated by the Brower algorithm to get a Delaunay triangulation. The main difference between such a mesh and the regular structured one is that the number of triangles each node belongs to is different. We also have done the same tests with regular meshes, and we have not seen any degradation of the convergence.

The locally smooth function we have chosen is obtained by a modification of that used by Harten in [11] for example : if ϕ is any angle, let f_ϕ be :

$$f_\phi(x,y) = \begin{cases} \text{if } r \le -\frac{1}{3},\ f_\phi(x,y) = -r\sin(\frac{\pi}{2}r^2), \\ \text{if } r \ge \frac{1}{3},\ f_\phi(x,y) = 2r - 1 + \frac{1}{6}\sin(3\pi r), \\ \text{if } |r| < \frac{1}{3},\ f_\phi(x,y) = |\sin(2\pi r)|, \end{cases} \quad \text{where } r = x + \tan(\phi)y, \tag{38}$$

and let u be :

$$\begin{cases} \text{if } x \le \frac{1}{2}\cos\pi y,\ u(x,y) = f_{\sqrt{\pi/2}}(x,y), \\ \text{if } x > \frac{1}{2}\cos\pi y,\ u(x,y) = f_{-\sqrt{\pi/2}}(x,y) + \cos(2\pi y). \end{cases} \tag{39}$$

The function defined by (38)-(39) shows discontinuities in the function itself and its first order derivatives; some of the discontinuities are straight lines (never aligned to the mesh), one is a curved line where the jump changes from one point to another. Last, the behavior of u is basically one-dimensional on the left of the curve $x = \cos\pi y/2$ and really two-dimensional on the right.

A plot of this function is given in Figure 9. One should obtain straight lines and smooth discontinuity transitions contrary to what is shown in the Figure : this is an effect of the graphic device adapted to P_1 interpolation.

Third order interpolation and reconstruction We have displayed in Figure 10 the L^∞ error of the interpolation for the smooth test case. The plain curve with squares is obtained with the E.N.O. interpolation, the plain curve with circles is obtained with the E.N.O. reconstruction. The dashed line indicates the slope -3. One can see that the expected order of accuracy is indeed reached.

In Figures 12-(a) and 13-(a), we have displayed the node values of the E.N.O. reconstruction for two meshes (1600 nodes and 6400 nodes). To better see the behavior of the approximation technique, we also present cross-subsection on three lines : $Y = 0.75$, $Y = 0$ and $Y = -0.45$ (Figures 14, 15 and 16. The approximations are obtained from the 1600 nodes mesh (see Figure 8). The latter line goes through one of the triple points (see Figure 9). One can see that the various discontinuities and the smooth regions are well captured by both techniques.

In [13], another selection procedure has also been proposed. It includes a much richer choice of stencil but no real improvement has been noticed. From all our experiments, we can conclude that this choice is indeed sufficient.

Fourth order interpolation and reconstruction The same tests have been performed for the fourth order interpolation and reconstruction of the smooth function. The Figure 11 shows the L^∞ error of the ENO reconstruction for random meshes. The Figures 12-(b) and 13-(b) shows an overall picture of the fourth order ENO reconstruction. A better capture of the area surrounding the triple points is the only visible difference between third and fourth order reconstruction.

To end this subsection, we must note that the algorithm for choosing the stencils may lead to some difficulties at the boundaries as can be seen in Figure 9 on the left upper corner : the most left upper triangle of the mesh (Figure 8) does not admit any additional points of the type we consider to make a stencil.

9 A class of high order numerical scheme for compressible flow simulations

9.1 The Euler equations

Let us quickly recall elementary things about the Euler equation of a calorically perfect gas :

$$\frac{\partial W}{\partial t} + \frac{\partial F(W)}{\partial x} + \frac{\partial G(W)}{\partial y} = 0 \tag{40}$$

As usual, in equation (40), W stands for the vector of conserved quantities and F (respectively G) is the flux in the x direction (resp. y direction) :

$$W = \begin{pmatrix} \rho \\ \rho u \\ \rho v \\ E \end{pmatrix} \quad F(W) = \begin{pmatrix} \rho u \\ \rho u^2 + p \\ \rho uv \\ u(E+p) \end{pmatrix} \quad G(W) = \begin{pmatrix} \rho v \\ \rho uv \\ \rho v^2 + p \\ v(E+p) \end{pmatrix} \tag{41}$$

with initial and boundary conditions. In equation (41), ρ is the density, u, v are the components of the velocity, E is the total energy and p the pressure, related to the conserved quantities by the

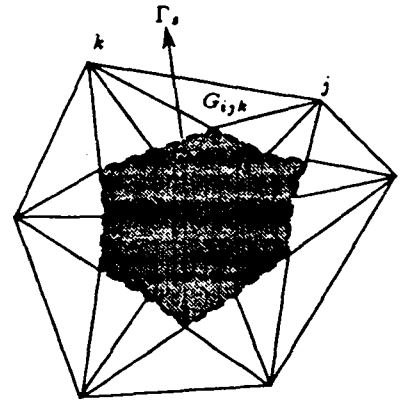

Figure 7: Element of the dual mesh

equation of state :

$$p = (\gamma - 1)\left(E - \frac{1}{2}\rho(u^2 + v^2)\right) \tag{42}$$

The ratio of specific heats, γ, is kept constant.

It is well known that the system defined by equations (40), (41) and (42) is hyperbolic : for any vector $\vec{n} = (n_x, n_y)$, the matrix :

$$A_{\vec{n}} = n_x \frac{\partial F}{\partial W} + n_y \frac{\partial G}{\partial W} \tag{43}$$

is diagonalizable and has real eigenvalues and eigenvectors. Let us describe now the construction of a k th order scheme.

9.2 Finite volume formulation

We consider a mesh $\mathcal{M}$ and the control volumes as on figure 7. The semi discrete finite volume formulation of (40) is :

$$\frac{\partial}{\partial t}\overline{W}_i(t) = -\frac{1}{area(\mathcal{C}_i)}\int_{\partial \mathcal{C}_i} \mathcal{F}_{\vec{n}}[W(x,t)]dl = \mathcal{L}_i(t) \tag{44}$$

Here, $W(t)$ is the (spatial) mean value of $W(x,t)$ at time t over $\mathcal{C}_i$, $\vec{n} = (n_x, n_y)$ is the outward unit normal to $\partial \mathcal{C}_i$, and $\mathcal{F}_{\vec{n}} = n_x F + n_y G$. We first describe the spatial approximation of (44), then the temporal discretization of the resulting set of ordinary differential equations. Last, we detail the boundary conditions.

9.2.1 Spatial discretization

For the sake of simplicity, we define the integer number p such that either $k = 2p$ or $k = 2p + 1$. The first step is to discretize $\mathcal{L}_i(t)$ up to k^{th} order. First, we can rewrite $area(\mathcal{C}_i)\mathcal{L}_i(t)$ as :

$$\int_{\partial \mathcal{C}_i} F_{\vec{n}}[W(x,t)]dl = \sum_{\Gamma_e} \int_{\Gamma_e} F_{\vec{n}}[W(x,t)]dl \tag{45}$$

where, as on figure 7, the set of the Γ_s's is that of the linear edges of C_i. On each Γ_s, $\vec{n}$ is constant. We consider, on any Γ_s, the p Gaussian points $\{G_l\}_{1\leq l\leq p}$ associated to the Gaussian formula of order $2p+1$. The integral $\int_{\Gamma_s} F_{\vec{n}}[W(x,t)]dl$ is approximated by

$$\sum_{l=1}^{p} \omega_l \mathcal{G}_{\vec{n},l}(t) \tag{46}$$

where term $\mathcal{G}_{\vec{n},l}(t)$ is defined now. Set C_j the other control volume of which Γ_s is a part of the boundary. In C_i and C_j , one compute the ENO reconstructions at time t of W, $R_i[W(\ .\ ,t),k]$ and $R_j[W(\ .\ ,t),k]$, up to order k. The ENO reconstruction of section 7 is applied to the physical variables, then one deduce the conserved ones. From that, we set, in equation (46) :

$$\mathcal{G}_{\vec{n},l}(t) = \mathcal{F}_{\vec{n}}^{\text{Riemann}}\{R_i[W(\ .\ ,t),k](G_l), R_j[W(\ .\ ,t),k](G_l)\}. \tag{47}$$

In equation (47), $\mathcal{F}_{\vec{n}}^{\text{Riemann}}$ may be any of the available Riemann solvers. In all the example below, we have chosen Roe's Riemann solver with Harten-Hyman entropy correction.

9.2.2 Temporal discretization

The equations (44), (45), (46) and (47) defines a finite set of ordinary differential equations that we symbolize by

$$\frac{\partial}{\partial t}\overline{W}_i(t) = \tilde{\mathcal{L}}_i(t) \tag{48}$$

In (48), $\tilde{\mathcal{L}}_i(t)$ is the discrete version of $\mathcal{L}_i(t)$. This equation is discretized by the k^{th} order version of the Runge-Kutta scheme of Shu [10] :

$$\begin{cases} W_i^{(l)} = \sum_{m=0}^{l-1}[\alpha_{lm}W_i^{(m)} + \beta_{lm}\tilde{\mathcal{L}}_i^{(m)}], \quad l = 1,2,\cdots,p, \quad \tilde{\mathcal{L}}_i^{(m)} = \tilde{\mathcal{L}}_i(W_i^{(m)}) \\ W_i^{(0)} = W_i^n, \qquad\qquad W_i^{(p)} = W_i^{n+1}. \end{cases} \tag{49}$$

The order of accuracy, as well as its TVD properties, is achieved by adequate sets of coefficients α_{lm}, β_{lm} and p (see [10] for details).

9.2.3 Boundary conditions

Let Γ be the boundary of the computational domain and $\vec{n}$ be the outward normal unit on Γ. We assume that Γ is divided into two parts, $\Gamma = \Gamma_0 \cap \Gamma_\infty$, on which different boundary conditions will be used. Here, Γ_0 represents a solid wall while Γ_∞ represents the far-field (inflow or outflow).

We do not treat a boundary condition by forcing the value of a variable to a prescribed boundary value, but consider instead the integral formulation (44) and apply boundary condition by modifying the flux integrals on ∂C_i for those cells such that $\Gamma \cap \partial C_i \neq \emptyset$.

For example, for a vertex i located on Γ_0, we do not impose the slip condition $\vec{U}.\vec{n} = 0$ but take this condition into account in the evaluation of the convective flux :

$$\int_{\Gamma_0\cap\partial C_i} Fn_x + Gn_y = \begin{bmatrix} 0 \\ \int_{\Gamma_0\cap\partial C_i} pn_x \\ \int_{\Gamma_0\cap\partial C_i} pn_y \\ 0 \end{bmatrix}.$$

The pressure integrals are computed as :

$$\int_{\Gamma_0 \cap \partial C_i} p n_x \simeq p_i \int_{\Gamma_0 \cap \partial C_i} n_x, \qquad \int_{\Gamma_0 \cap \partial C_i} p n_y \simeq p_i \int_{\Gamma_0 \cap \partial C_i} n_x.$$

For a vertex located on Γ_∞, we again use an approximate Riemann solver. We define a far field state W_∞, $\vec{n}_i = \int_{\Gamma_\infty \cap \partial C_i} \vec{n}$ and set, in agreement with what has been done in the interior of the computational domain

$$\int_{\Gamma_\infty \cap \partial C_i} F n_x + G n_y = \Phi(W_i, W_\infty, \vec{n}_i). \tag{50}$$

In equation (50), Φ is a numerical flux function. For simplicity reasons, we have chosen a modified Steger-Warming flux instead as the Roe one,

$$\Phi(W_i, W_\infty, \vec{n}) = A^+_{\vec{n}} W_i + A^-_{\vec{n}} W_\infty$$

The matrices $A^+_{\vec{n}}$ and $A^-_{\vec{n}}$ are the positive and negative parts of the matrix $A_{\vec{n}}$ defined in (43) and evaluated for $W = W_i$.

In all the examples we have treated below, the boundary where either fully subsonic or either fully supersonic, so that the procedure was really simple, contrarily to what would have appended in mixed type boundary condition.

Finally, we have reduced the order of accuracy of the reconstruction for cells that are too near from the boundary. For them, a proper calculation of the ENO stencil may be impossible because the set of possible stencil is biased in one direction due to the boundary. For the third order scheme, these cells are those related to a mesh point that belongs to a triangle having at least one point on the boundary. For the fourth order scheme, they are those belonging to a triangle a vertex of which is related to a cell for which a reduction of order must be done for third order.

9.3 Positivity of the density and the pressure

As pointed out by Harten et al. [24], in some situation and for extremely few cells, the ENO reconstruction of the density and pressure may lead to negative values. For these cells, and these cells only, following [24], we reduce the order of accuracy with the following inductive method (w is either the density or the pressure, w_i is its average on C_i). Consider, in C_i, the reconstruction

$$R[w, n](X, Y) = \sum_{l=0}^{n} \sum_{p+q=l} a_{pq} (X - x_g)^p (Y - y_g)^q,$$

If $\sum_{l=2}^{n} \sum_{p+q=l} |a_{pq}||(x - x_g)^p (y - y_g)^q| \geq \alpha |w_i|$ at a Gaussian point (x, y), then the reconstruction, for that point, is set to $R[w, n-1](x, y)$. Then, we repeat the test if necessary. Usually, the parameter α is set to 0.95.

In all the simulations we have done, the tests were positive for a very small set of cells and a zeroth order reconstruction was never used. They were never positive for the second order scheme. This number is problem dependent. For example, only at most three points caused problems from time to times for the facing step problem with a 5000 nodes mesh. They all were located in the front shock.

10 Numerical tests

All the example we propose now have been computed with the second and third ENO schemes. The ratio of specific heats, γ is always set to 1.4.

10.1 A Shock tube problem

We have set up a two dimensional shock tube problem in the square $[0,1]\times[0,1]$. Its boundary are solid. The initial conditions are :

$$\text{If } x \leq 0.5 \text{ and } |y-0.5| \leq 0.25, \quad \begin{cases} \rho = 1. \\ u = v = 0. \\ p = 1. \end{cases}$$

$$\text{else} \quad \begin{cases} \rho = 0.125 \\ u = v = 0. \\ p = 0.1 \end{cases}$$

The mesh is completely unstructured with 2127 nodes and 4088 triangles. The velocity field obtained by the third order scheme at time $t = 0.9$ is displayed in Figure 18.The differences between both results are more clearly visible in the near stagnation zone. In order to better represent that area, we have removed from the velocity field all the points for which the sum of the absolute values of its two components is larger than 0.15. The result is shown on Figures 19 (second order) and 20 (third order). One can clearly observes that the number of small structures of the flow is much more important in Fig. 20 than in Fig. 19. The shocks in the upper and lower part of the pictures have also a different resolution. Their location is also different but this can be seen only by superimposing the pictures.

One should also mention that this test is not particularly easy for our method. After a few time, the shock reflects with the wall. The reflected shock interacts with the others structures of the flow, leading to interactions between the various kind of discontinuities and with the smooth parts of the flow. The multiple points, as shown on our figures, with different kind of discontinuities (contact and shock) are resolved by our method without any particular trick.

10.2 A Mach 3 wind tunnel with a step

We have run this test case, that is well documented in [25], for the second order and third order ENO schemes on a 5140 nodes and 9958 triangles mesh. This discretization corresponds to the medium mesh used in [25]. A portion of it is displayed in Figure 21. It is totally unstructured. The conditions of the problem are the following : a uniform Mach 3 flow is set in a channel. At the initial time, a step of relative height 0.2 is installed in it. The channel length is 3 and the step is located at 0.6. This situation creates a shock that reflects on the upper part of the channel then it evolves to a lambda shock as the time increases. It interacts with the upper part of the step. A weak shock is also created by the expansion wave at the corner. This shock interacts with the reflected one creating a slip line. The location of this slip line is very dependent on the boundary conditions that are set at the corner.

Here, no special treatment is done, contrarily to what is advocated in [25], so that the quality of the second reflected shock is poor. We only want to verify the effect of the increasing order of

accuracy on the solution, so that we will only look at the first reflected shock. The solutions of Fig. 23 (second order ENO) and Fig. 24 (third order ENO) are shown. A clear improvement on the thickness of that reflected shock can clearly be seen from the horizontal cross section of the density at $y = 0.5$, Figure 22. The slip line coming from the lambda shock is also more visible in Figure 24 than in Fig. 23 as well as the weak shock near the corner.

10.3 Reflection of a shock on a wedge

This problem is also well documented in the literature. In order to achieve a correct solution, one has either to use very fine meshes or adapted meshes (see [6] for example). We have chosen a case where the planar shock enters from the left in a quiescent fluid. Its Mach number is $M_S = 5.5$ and is defined towards the flow values in the quiescent fluid where the density is set to 1.4 and the pressure to 1. One expects a double Mach reflection.

The mesh has only 8569 points and 16806 triangles. A part of it is shown in Figure 25. The density contours of the two calculations are displayed in Figures 26 (second order) and Figure 27 (third order). A very clear improvement of the slip line coming from the Mach stem can be observed. The second triple point can also been observed in Figure 27, though of poor quality because of the unsufficient resolution of the present mesh, but is totally undistinguishable in Figure 26. Generally speaking, all the discontinuities are better resolved by the third order scheme.

11 Conclusions and perspectives

In this lecture, we have tried to give an as broad as possible overview of ENO finite volume type schemes with much emphasis on the reconstruction problem, first for one-dimensional problems and then for multi-dimensional ones. We have also tried to give an as objective as possible opinion, in particular we have shown some of their problems and possible ways to solve them.

A third order ENO scheme has been derived on triangular type unstructured meshes ; this demonstrates that deriving ENO schemes on unstructured meshes is something possible. We indicate how to build higher order ENO schemes and give some comments on the numerical stability of the reconstruction step.

This new scheme has been tested on a set of well known test cases and compared to a second order one. In all cases, the results are clearly improved. Our results also demonstrates its robustness. The cost of the scheme is 4 times that of the second order one (on a Cray YMP) but the code is far from being optimized. In particular, no effort has been done in the ENO reconstruction procedure, the most expensive routine by far, so that this ratio can be considered as a bad upper bound. Last, this present version is fully upwinded, so that we have not yet taken into account the results of section 5.1 and following.

In the near future, we will derive the fourth order version of this class of schemes. The hybridization with central schemes will be studied. The two schemes will be coupled with a dynamic adaptation procedure [4] to improve its efficiency. Last, improvement of the Riemann solver has to be done : up to now, they assume a one-dimensional structure of the waves (material and acoustic). This is a crude approximation (see [33] for a review and the references therein). We intend to couple the new genuinely multidimensional Riemann of [34] with our fully multidimensional ENO procedure or to adapt the ideas of [35] with this ENO method.

References

[1] H.C. Yee. *Upwind and Symmetric Shock-Capturing Schemes.* Technical Report-TM-89464, NASA, May 1987, unpublished.

[2] L. Fezoui & B. Stoufflet. A Class of Implicit Upwind Schemes for Euler Simulations with Unstructured Meshes. *Journal of Computational Physics*, 84(1) pp : 174-206, September 1989.

[3] B. N'Konga & H. Guillard. Godunov type methods on non-structured meshes for tridimensional moving boundary problems, INRIA Report, to appear.

[4] N. Maman & B. Larrouturou. Dynamical mesh adaptation for two-dimensional reactive flow simulation, *Numerical Grid Generation in Computational Fluid Dynamics and Related Field*, S.-Arcilla, A. and Häuser, J. and Eiseman, P. R. and Thompson, J. F. Eds, Elsevier Science Publishers B. V., pp. 13-26, 1991

[5] B. Palmerio & A. Dervieux. The Capture of Viscous Layers by Non-Structured Mesh Deformation 13 th IMACS World Congress on Computation and Applied Mathematics, July 22, 26 1991, Dublin Ireland, To appear.

[6] J. J. Quirk. An Alternative to Unstructured Grids for Computing Gas Dynamic Flows around Arbitrarily Complex Two-Dimensional Bodies. Icase Report 92-7, February 1992.

[7] A. Harten & S. Osher. Uniformly High-Order Accurate Nonoscillatory Schemes-I, *SIAM Journal of Numerical Analysis*, Vol. 24, No 2, April 1987, pp. 279-309.

[8] A. Harten, S. Osher, B. Engquist & S. R. Chakravarthy. Some Results on Uniformly High-Order Accurate Essentially Nonoscillatory Schemes, Applied Numerical Analysis 2 (1986), pp. 347-377, Elsevier Science Publishers B.V (North Holland).

[9] A. Harten, B. Engquist, S. Osher & S. R. Chakravarthy. Uniformly High Order Accurate Essentially Non-Oscillatory Schemes III, *Journal of Computational Physics*, Vol 71, pp. 231-303. (1987).

[10] C.W. Shu & S. Osher. Efficient Implementation of Essentially Non-Oscillatory Shock-Capturing Schemes, *Journal of Computational Physics*, Vol 77, pp.439-471 (1988).

[11] A. Harten. ENO Schemes with Subcell Resolution, *Journal of Computational Physics*, Vol 83, pp.148-184 (1989).

[12] J. Casper & H.L. Atkins. A Finite-Volume Application of High Order ENO Schemes for Two-Dimensional Hyperbolic Systems, Submitted to the *Journal of Computational Physics.*

[13] R. Abgrall. Design of an Essentially Non-Oscillatory Reconstruction procedure on Finite-Elements type meshes, Icase report 91-84 (December 1991), in revised form INRIA Report No 1592 (January 1992), submitted to Math. of Comp.

[14] R. Abgrall. An Essentially Non Oscillatory Scheme on Unstructured Meshes, Proceedings of the Second International Conference on High Order and Spectral Methods, June 22-26, 1992. To appear as a special issue of *Computer Methods in Applied Mechanics and Engineering*, Elsevier, 1992

[15] A. Harten & S.R. Chakravarthy. Multi-Dimensional ENO Schemes for General Geometries, Icase Report No 91-76, September 1991, submitted to the Journal of Computational Physics.

[16] P. Vankeirsblick & H. Deconinck. Higher Order Upwind Finite Volume Schemes with ENO-properties for General Unstructured Meshes Paper No 7, AGARD R-787, May 1992, unpublished.

[17] T. J. Barth & P.O. Frederickson. High Order Solution of the Euler Equations on Unstructured Grids using Quadratic reconstruction, AIAA Paper No 90-0013, 28 th Aerospace Science Meeting, January 8-11, Reno, Nevada, unpublished.

[18] K.C. Chung & T. H. Yao. On Lattrices Admitting Unique Lagrange Interpolations, SIAM Journal of Numerical Analysis, Vol 14, No 4, September 1977, pp. 735–743.

[19] G. Muhlbach. The General Recurrence Relation for Divided Differences and the General Newton-Interpolation-Algorithm with Applications to Trigonometric Interpolation. Numerische Mathematik, Vol 32, pp. 393–408, 1979.

[20] G. Muhlbach. The General Neville-Aitken-Algorithm and Some Applications. Numerische Mathematik, Vol 31, pp. 97–110, 1978.

[21] G. Strang & G. J. Fix. An analysis of the finite element method. Prentice-Hall INC.,Englewood Cliffs, N.J., 1973

[22] P.G. Ciarlet & P. A. Raviart. General Lagrange and Hermite interpolation in $\mathbb{R}^n$ with application to Finite Element Methods. *Archive for Rational Mechanics and Analysis*, Vol 42, 1972, pp. 177–199.

[23] A. Dervieux, L. Fezoui & F. Loriot. On high resolution extensions of the Lagrange-Galerkin finite-element schemes, INRIA Report, No 1703, June 1992.

[24] A. Harten, B. Engquist, S. Osher & S.K. Chakravarthy. Uniformly High Order Accurate Essentially Non-Oscillatory Schemes III, Icase Report 86-22, April 1986, unpublished.

[25] P. Woodward & Colella. The Numerical Simulation of Two-Dimensional Fluid Flow with Strong Shocks, *Journal of Computational Physics*, Vol 54, pp. 115–173, 1984

[26] P.G. Ciarlet & P. A. Raviart. General Lagrange and Hermite interpolation in $\mathbb{R}^n$ with application to Finite Element Methods. *Archive for Rational Mechanics and Analysis*, Vol 42, 1972, pp. 177-199.

[27] A. Harten. On the non linearity of modern shock capturing schemes, in *Wave Motion : Theory, Modelling and Computation*, Proceedings of a conference of the 60th birthday of P.D. Lax, Edited by A.J. Chorin and A.J. Majda ; Mathematical Sciences Research Institute Publications, Springer Verlag, pp 147-201, also ICASE Report 86-69, (1987)

[28] P. Vankeirsbilck. Algorithmic developments for the solution of hyperbolic conservation laws on adaptive unstructured grids PhD Thesis, Von Karmàn Institute, March 1993.

[29] E. Meiburg, A. Rogerson & C-W. Shu. A numerical study concerning the convergence of ENO schemes, (1990)

[30] F.C. Lafon & S. Osher. High order filtering methods for solving conservation laws, *Journal of Computational Physics*, 96, pp 110-142, (1991)

[31] J.A. Désideri & P.W. Hemcker. Analysis of convergence of iterative implicit and defect-correction algorithms to hyperbolic problems, INRIA Report No 1200, March 1990. Also submitted to SIAM.

[32] C-W. Shu. Numerical experiments on the accuracy of ENO and modified ENO schemes, To appear in *Journal of Scientific Computations.*

[33] B. van Leer. Progress in multi-dimensional upwind differencing, Icase report 92-43

[34] R. Abgrall. A genuinely multidimensional Riemann Solver, INRIA report No 1859, February 1993.

[35] F. Angrand & F.C. Lafon. Flux formulation using a fully 2D approximate Roe Riemann solver, Submitted to the *Journal of Computational Physics*

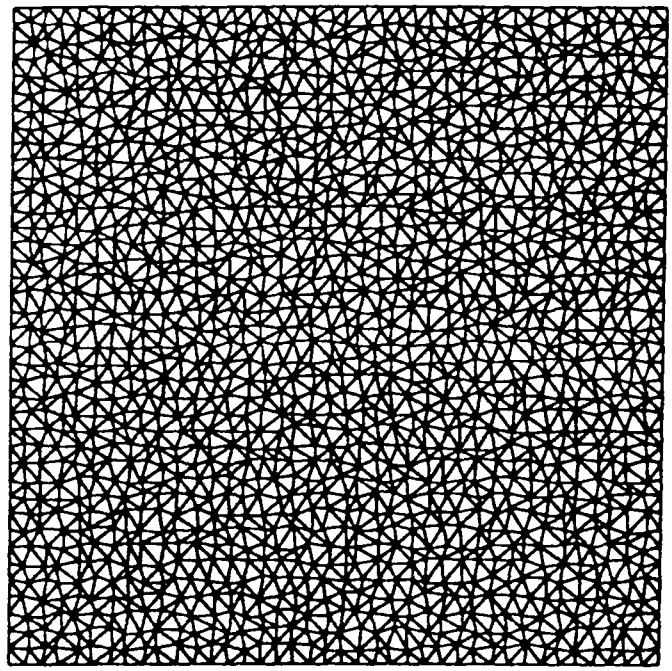

Figure 8: Typical mesh. 1600 nodes, 3042 triangles.

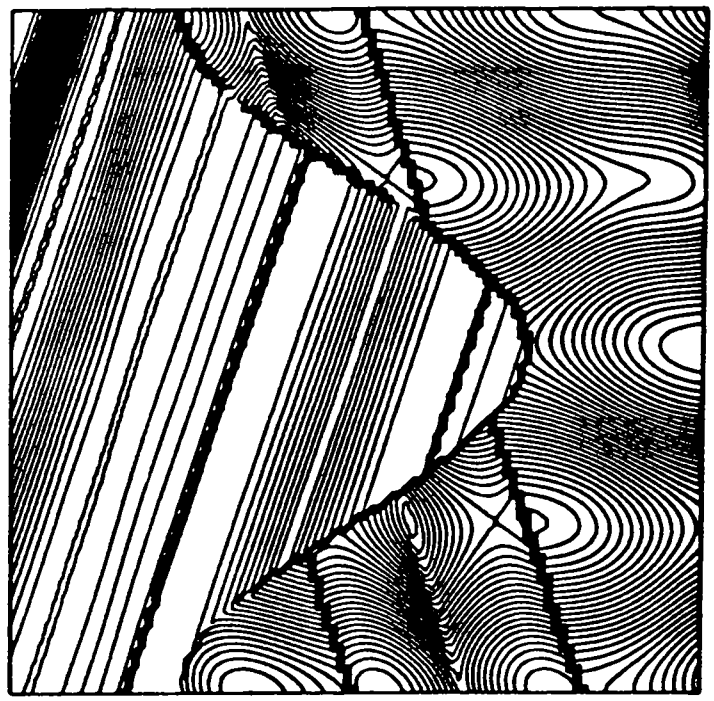

Figure 9: Exact function. Min=-1.331, Max=2.650, $\delta = 0.1$.

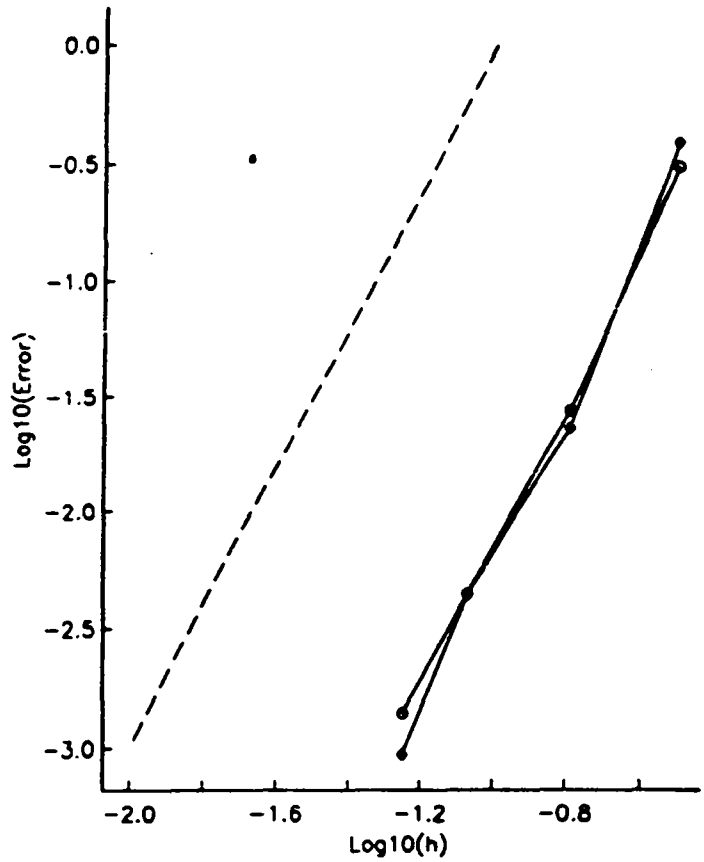

Figure 10: L^∞ error for $f(x,y) = \cos[2\pi(x^2+y^2)]$. Squares : E.N.O. interpolation only, Circles : E.N.O. + reconstruction. Dashed line : slope -3

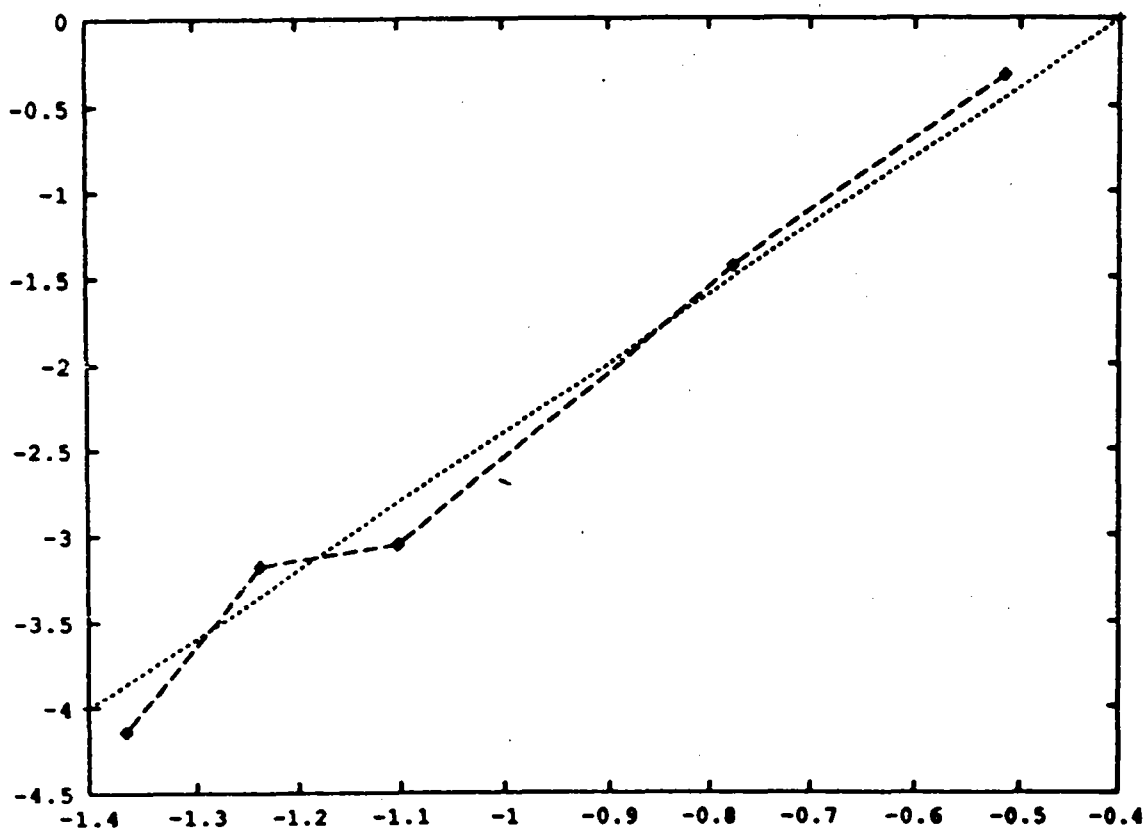

Figure 11: L^∞ error for $f(x,y) = \cos[2\pi(x^2+y^2)]$. Squares : Dashed line : slope -4, Dashed+squares : E.N.O. + reconstruction

(a) Third order

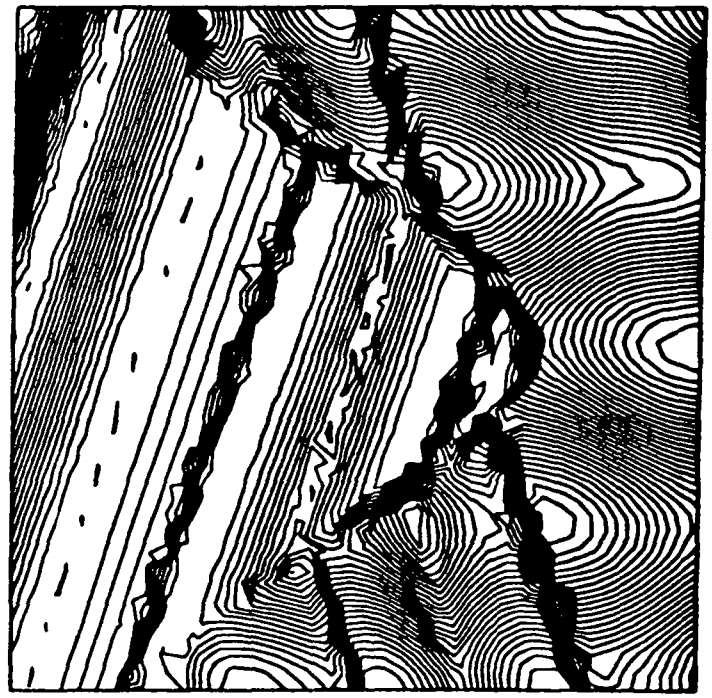

(b) Fourth order

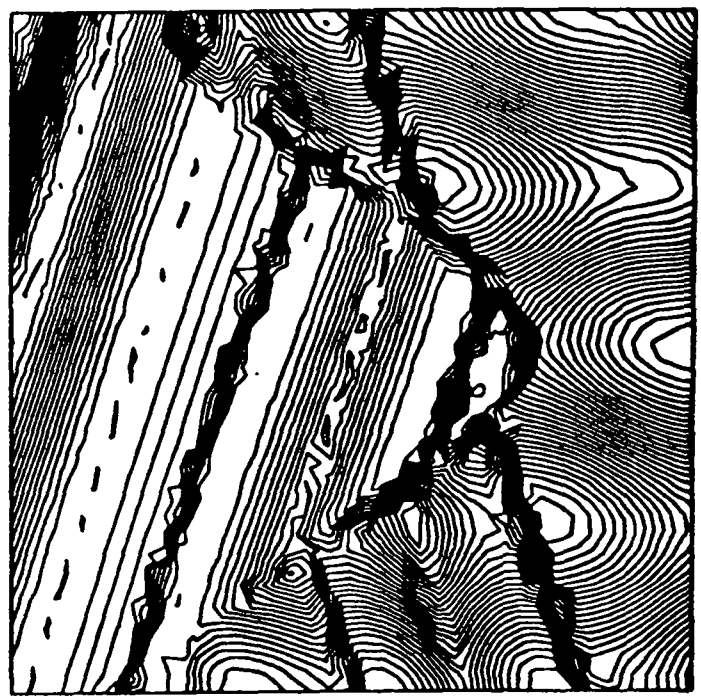

Figure 12: E.N.O. reconstruction "in the mean" with the 1600 nodes mesh. Min=-1.30, Max=2.6, $\delta = 0.1$.

(a) Third order

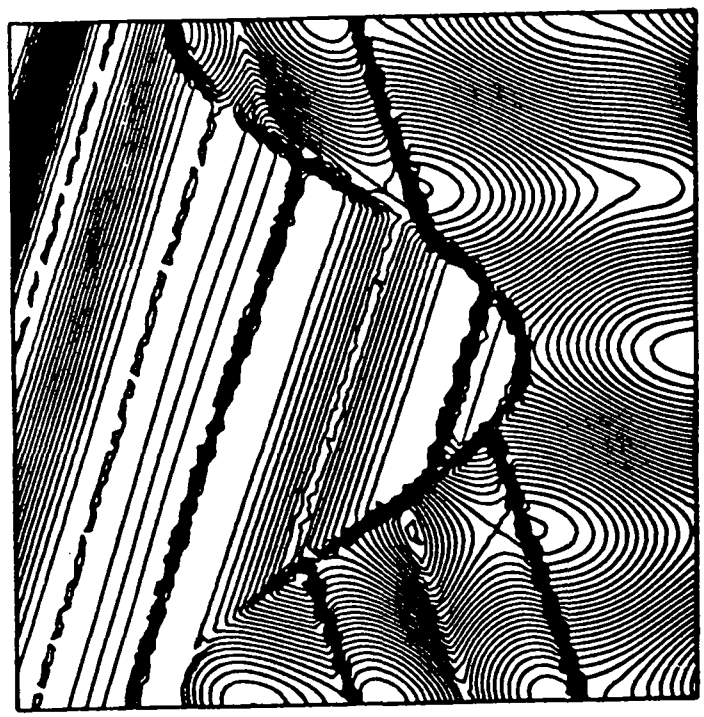

(b) Fourth order

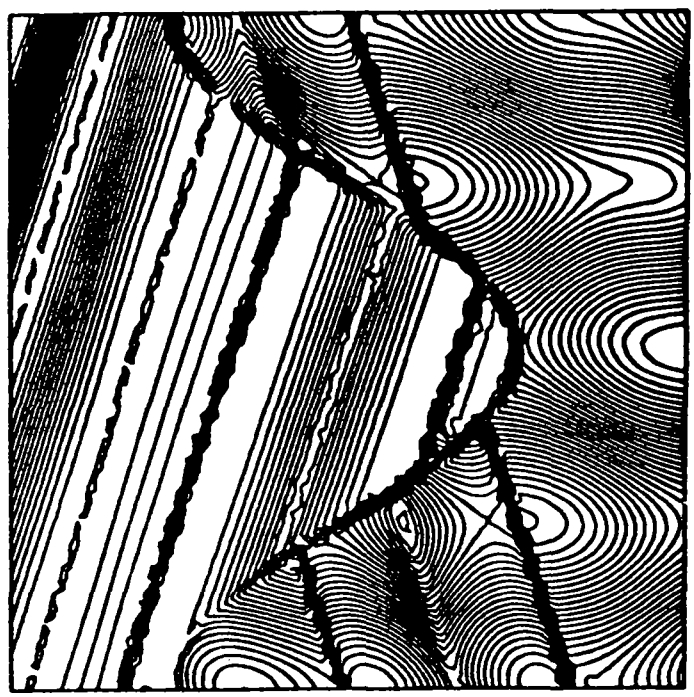

Figure 13: E.N.O. reconstruction "in the mean" with the 6400 nodes mesh. Min=-1.30, Max=2.6, $\delta = 0.1$.

(a) E.N.O. interpolation.

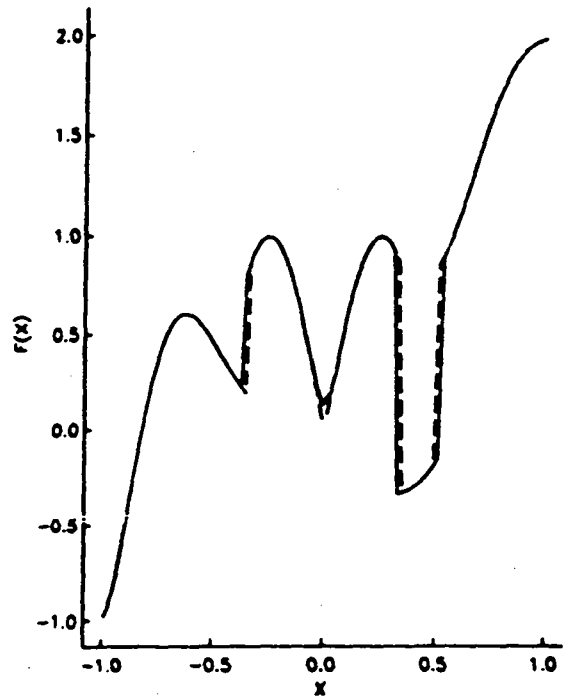

(b) E.N.O. reconstruction.

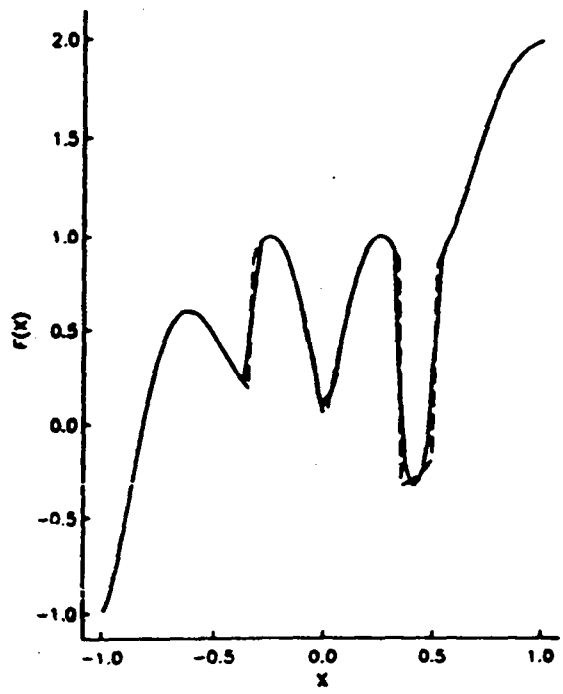

Figure 14: Cross-subsection at $Y = 0$ of the E.N.O interpolation (a) and the E.N.O. reconstruction (b) for 1600 nodes the mesh.

(a) E.N.O. interpolation.

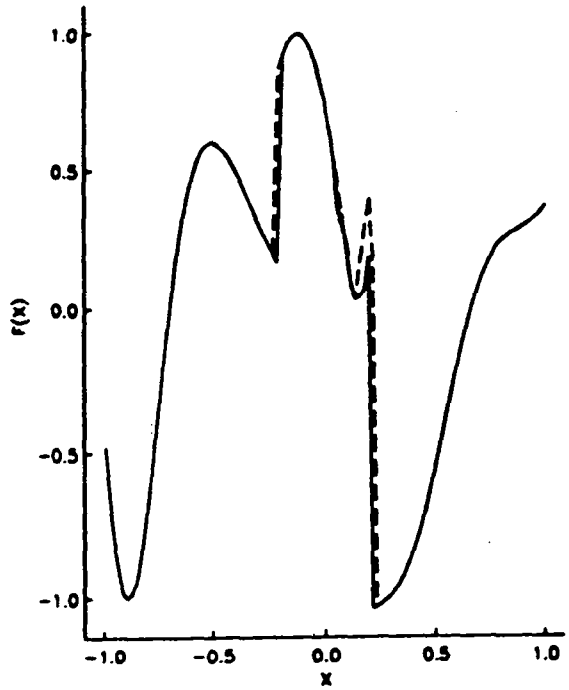

(b) E.N.O. reconstruction.

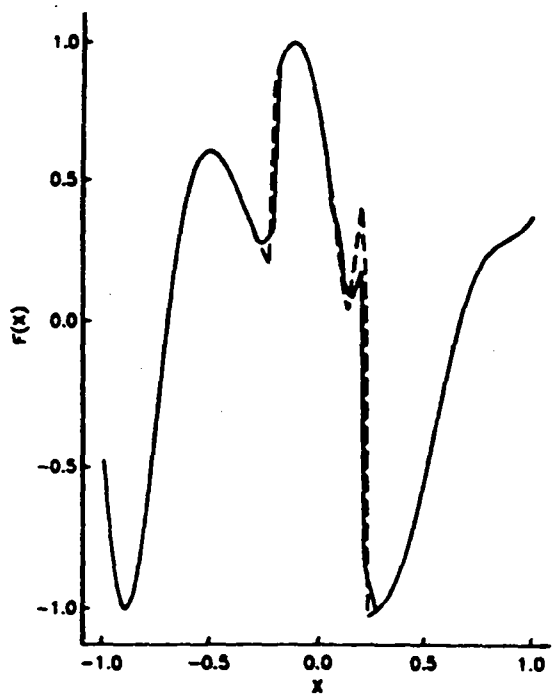

Figure 15: Cross-subsection at $Y = 0.75$ of the E.N.O interpolation (a) and the E.N.O. reconstruction (b) for the 1600 nodes mesh.

(a) E.N.O. interpolation.

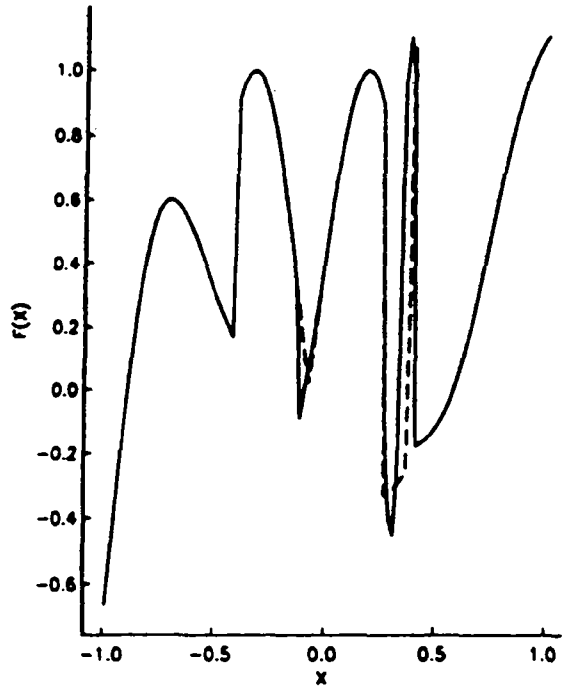

(b) E.N.O. reconstruction.

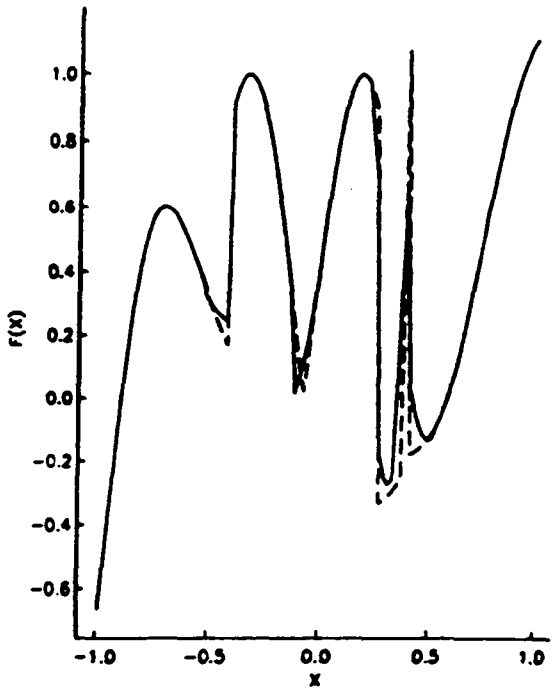

Figure 16: Cross-subsection at $Y = -0.45$ of the E.N.O interpolation (a) and the E.N.O. reconstruction (b) for the 1600 nodes mesh.

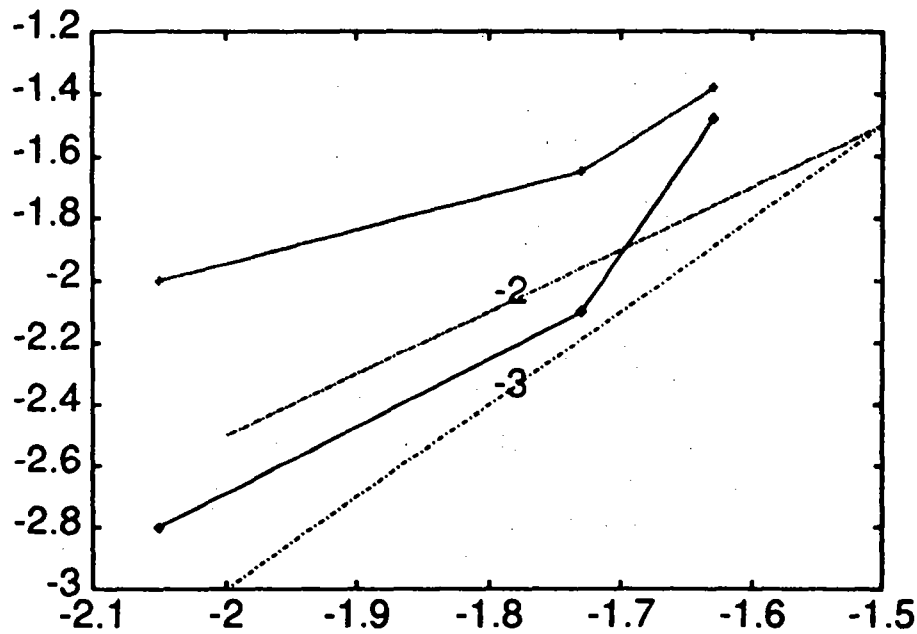

Figure 17: Representation of the logarithm of the L_∞ error in term of the logarithm of the maximum radius of the circumcircles.

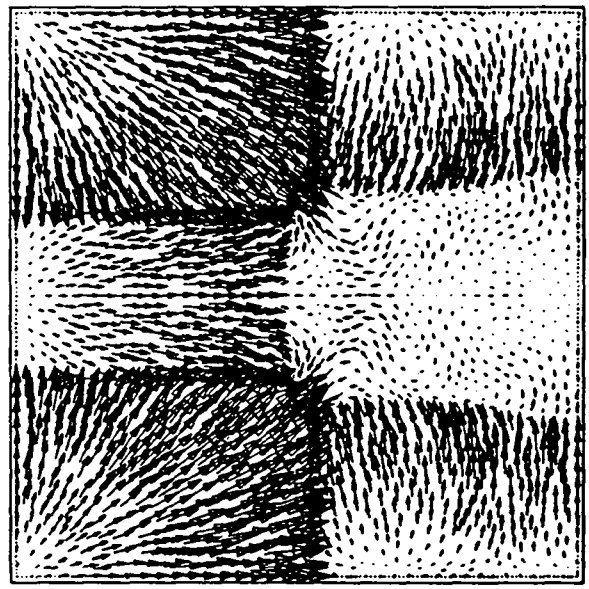

Figure 18: Shock tube : velocity field at time $t = 0.9$

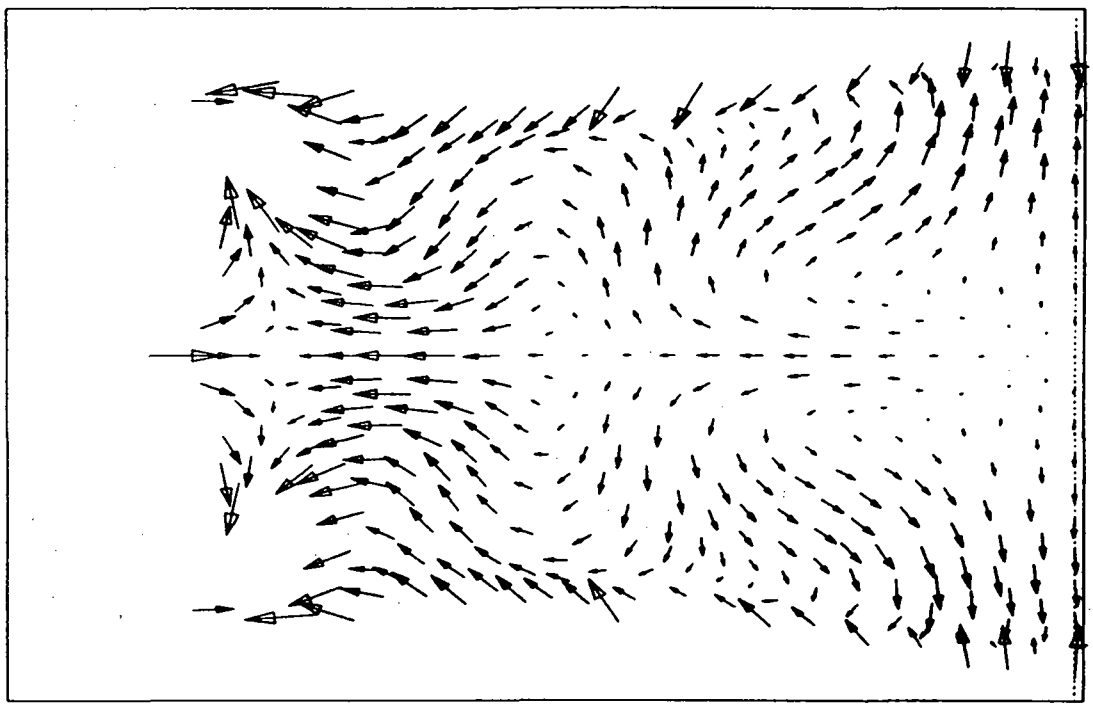

Figure 19: Zoom of the velocity field in $[0.5, 1] \times [0.25, 0.75]$. Second order solution

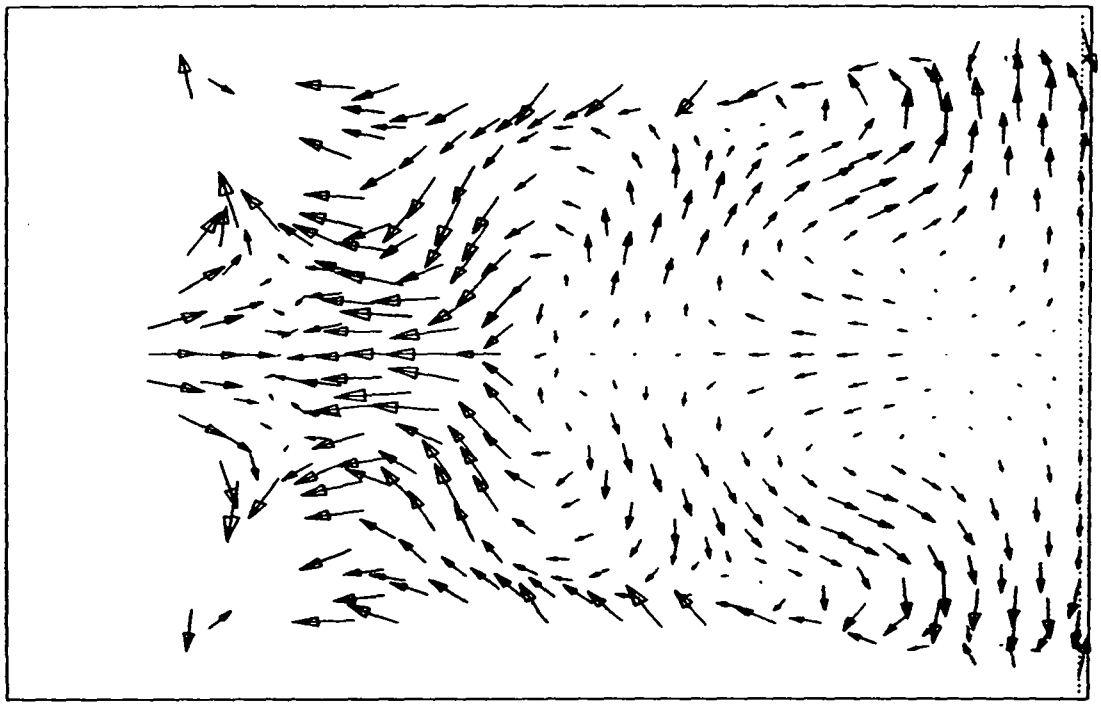

Figure 20: Zoom of the velocity field in $[0.5, 1] \times [0.25, 0.75]$. Third order solution

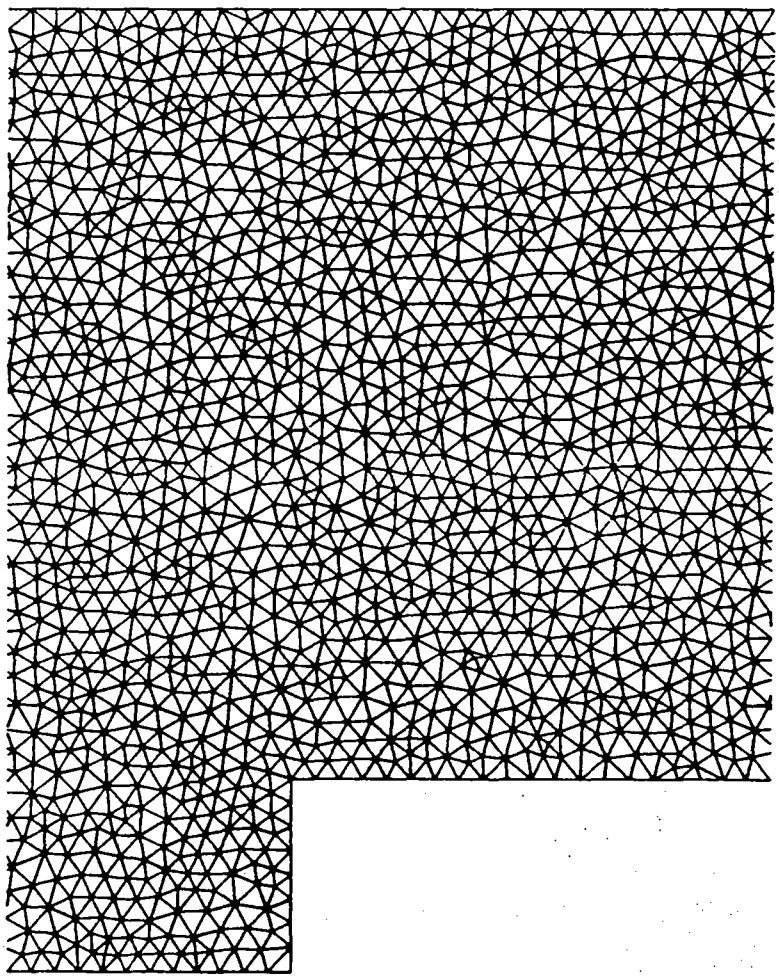

Figure 21: Portion of the mesh used for the step case

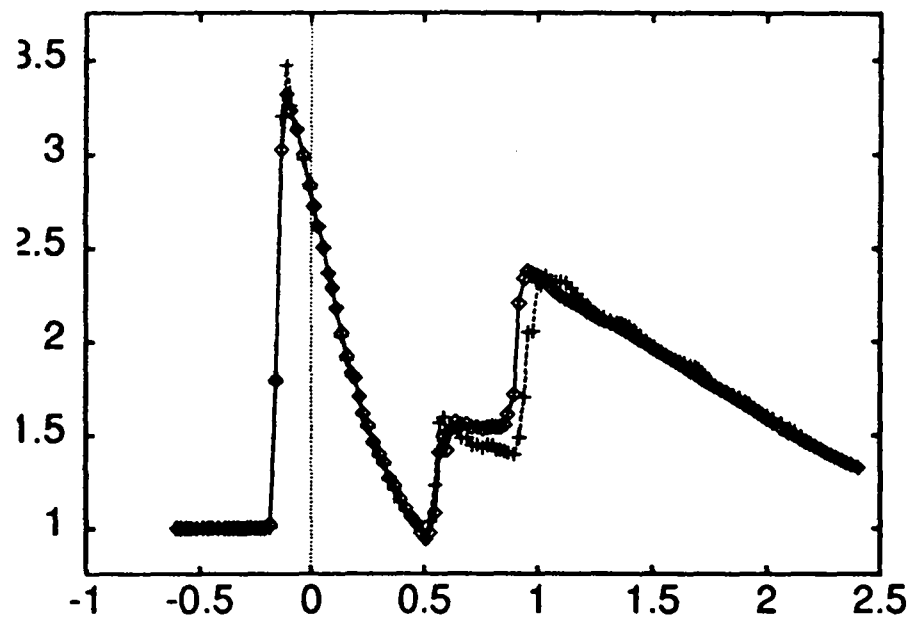

Figure 22: Cross-section of the density, $y = 0.5$ $\diamond$: second order, $+$: third order

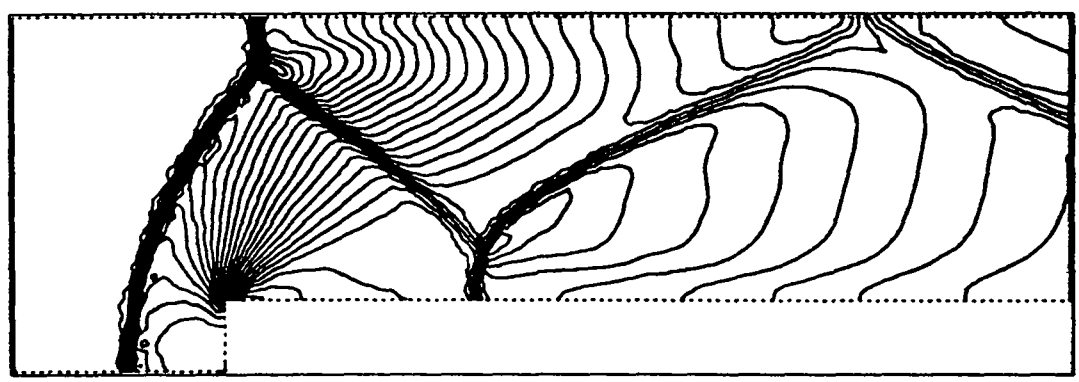

Figure 23: Density contours for the second order ENO solution, t=4, min=0.329, max=4.64. Density contours from 0.287 to 4.584, $\Delta\rho = 0.14$

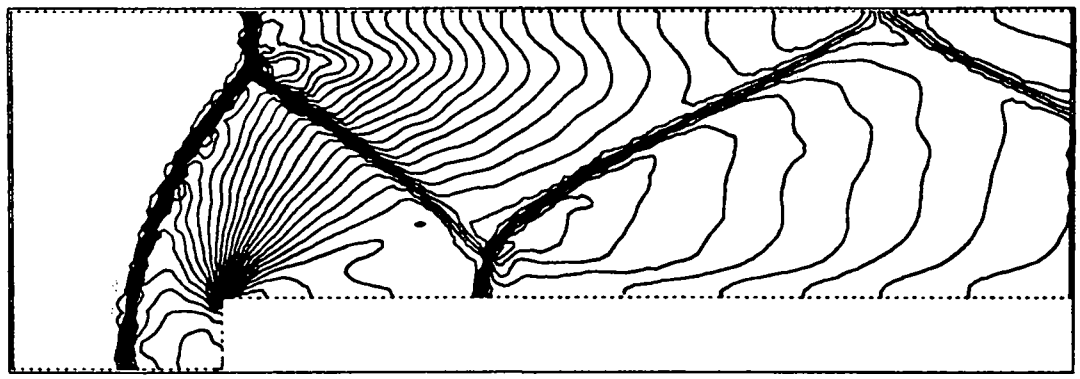

Figure 24: Density contours for the third order ENO solution, t=4, min=0.287, max=4.584, $\Delta\rho$ = 0.14

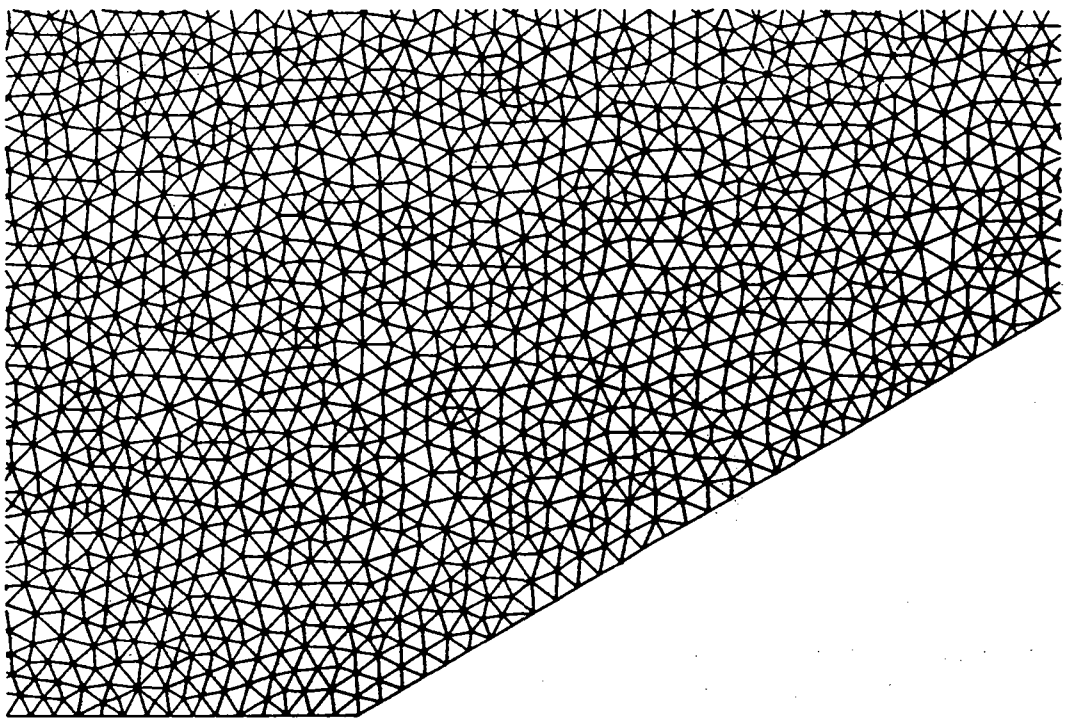

Figure 25: Portion of the mesh used for the Mach reflection problem

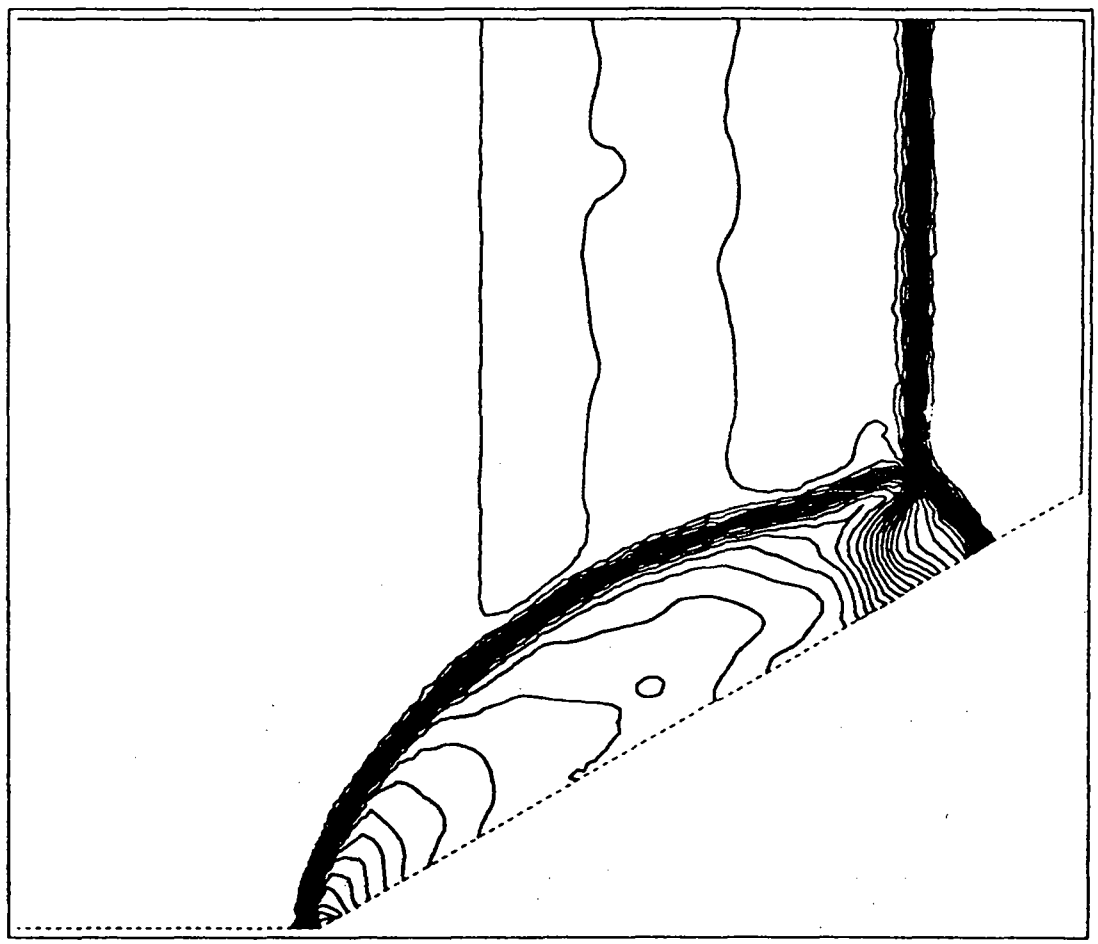

Figure 26: Refection of a planar shock by a wedge : density contours, second order solution. Min=1.4, Max=17.3. Contour from 1.4 to 19.088, $\Delta\rho = 0.36$

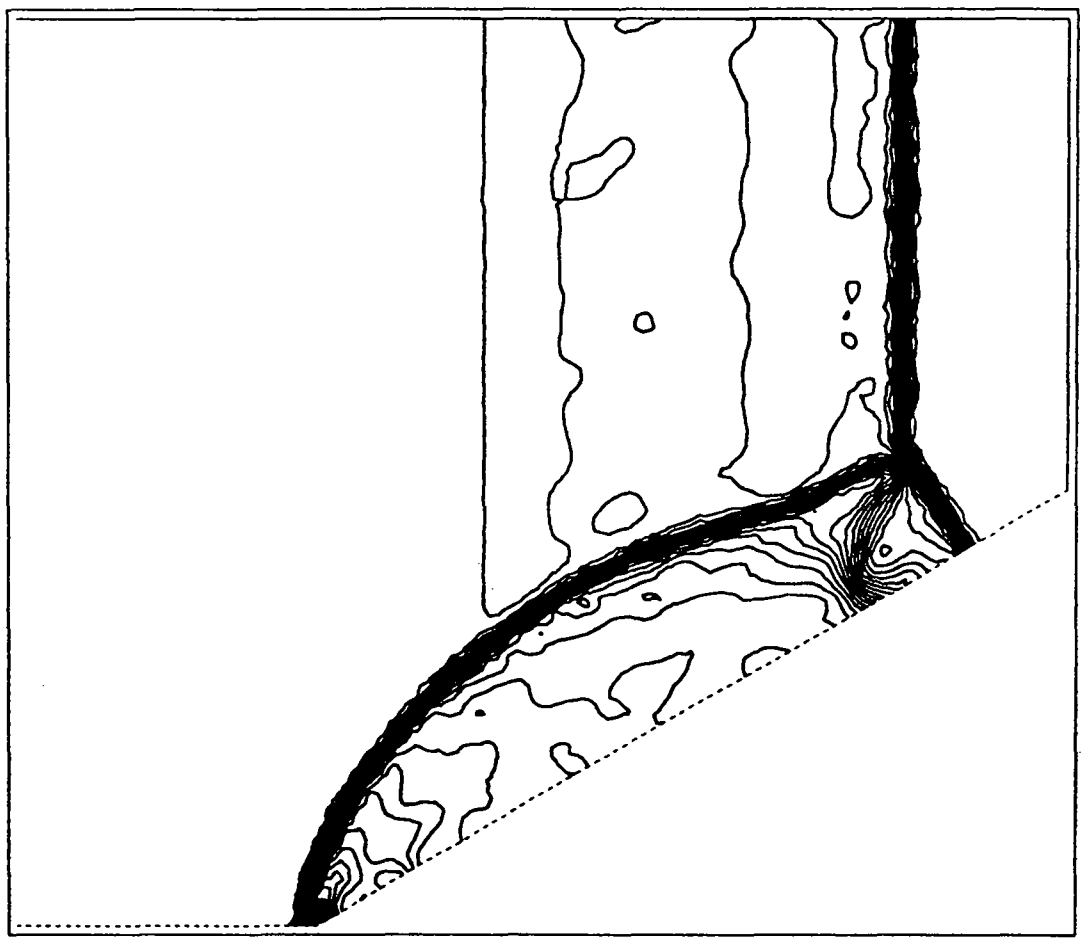

Figure 27: Refection of a planar shock by a wedge : density contours, third order solution. Min=1.4, Max=19.088, $\Delta\rho = 0.36$

Unité de Recherche INRIA Sophia Antipolis
2004, route des Lucioles - B.P. 93 - 06902 SOPHIA ANTIPOLIS Cedex (France)

Unité de Recherche INRIA Lorraine Technopôle de Nancy-Brabois - Campus Scientifique
615, rue du Jardin Botanique - B.P. 101 - 54602 VILLERS LES NANCY Cedex (France)
Unité de Recherche INRIA Rennes IRISA, Campus Universitaire de Beaulieu 35042 RENNES Cedex (France)
Unité de Recherche INRIA Rhône-Alpes 46, avenue Félix Viallet - 38031 GRENOBLE Cedex (France)
Unité de Recherche INRIA Rocquencourt Domaine de Voluceau - Rocquencourt - B.P. 105 - 78153 LE CHESNAY Cedex (France)

EDITEUR
INRIA - Domaine de Voluceau - Rocquencourt - B.P. 105 - 78153 LE CHESNAY Cedex (France)

ISSN 0249 - 6399